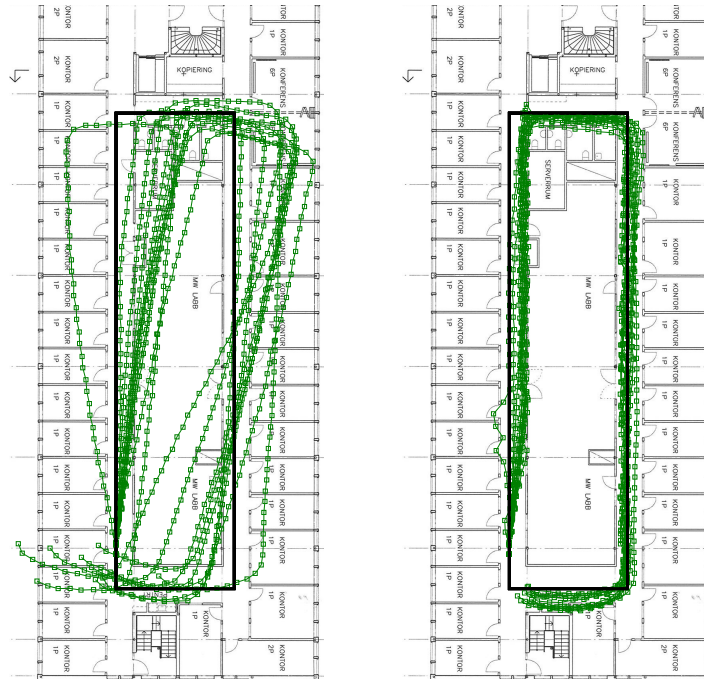


CHALMERS



INDOOR POSITIONING FOR MOBILE DEVICES USING
INSTRUMENTATION AND DEAD RECKONING

MASTER'S THESIS

JONATAN O. ERIKSSON

L. HAMPUS TENGFJORD

Department of Signals and Systems

CHALMERS UNIVERSITY OF TECHNOLOGY

Göteborg, Sweden

EX036/2014

Master's Thesis EX036/2014

Indoor Positioning for Mobile Devices
using Instrumentation and Dead
Reckoning

Jonatan O. Eriksson
L. Hampus Tengfjord

Department of Signals and Systems
CHALMERS UNIVERSITY OF TECHNOLOGY
Gothenburg, Sweden 2014

Indoor Positioning for Mobile Devices using Instrumentation and Dead Reckoning
Jonatan O. Eriksson
L. Hampus Tengfjord

© Jonatan O. Eriksson, L. Hampus Tengfjord, 2014

Master's Thesis EX036/2014
Department of Signals and Systems
CHALMERS UNIVERSITY OF TECHNOLOGY
SE-412 96 Göteborg
Sweden
Telephone + 46 (0)31-722 1000

Cover:
Trajectories about the office floor of Ascom using the Complementary filter described
in the report.

Chalmers University of Technology
Göteborg, Sweden 2014

Aire, and ye Elements the eldest birth
Of Natures Womb, that in quaternion run
Perpetual Circle, multiform; and mix
And nourish all things, let your ceaseless change
Varie to our great Maker still new praise.
-John Milton, Paradise Lost

Abstract

The recent surge in popularity of Smart Phones and other mobile devices equipped with *inertial sensors* has made *Indoor Positioning* a hot research area. This report covers the conception, implementation, and evaluation of a *Pedestrian Dead Reckoning System*. Such systems often serve as bases for *Indoor Positioning Systems* which are used to track persons, vehicles, or goods inside indoor spaces. A Pedestrian Dead Reckoning system provides an estimate of trajectories walked by pedestrians. They do so by manipulating measurements of the accelerations and angular rates the device is subjected to. The system is intended to be used in conjunction with other systems that provide information about the absolute position such as networks of IR-beacons or Wifi-devices.

The system's purpose is to produce good positional estimates for mobile devices placed in the pocket. For the system to work under such circumstances, its orientation has to be estimated. A *quaternion* representation of the orientation is used for its many advantages. The orientation estimation is done by fusing data from gyroscopes and accelerometers. Three different filters are evaluated for the fusion, two types of *Extended Kalman Filters* and one *Complementary Filter*. One of the Kalman Filters uses a *Gauss-Newton* iteration algorithm to convert measurements of the acceleration to quaternion form. A part of the orientation, the *tilt*, is used by a separate step detection and step length estimation algorithm. The remaining part of the orientation, the *heading*, is combined with the step information to produce the trajectory. Additionally, a *mapping algorithm*, is created and added on top of the dead reckoning algorithms to further improve the accuracy of the system. It exploits knowledge of the physical surroundings in which the person moves about. This information is used to correct drift in position and heading.

The average error in position during 80 meter walks inside an office building without the mapping algorithm was 1.6 meters. With the mapping algorithm that error was reduced to 0.52 meters.

KEYWORDS: Inertial Navigation, Indoor Positioning, Pedestrian Dead Reckoning, Quaternions, Indoor Environment, Kalman Filters, Map-Matching, Motion Measurements

Acknowledgments

We would like to thank Ascom for giving us the opportunity to carry out this thesis project, Lennart Svensson of Chalmers University of Technology for being our examiner, and Fredrik Gustafsson of The Institute of Technology at Linköping University for helping us getting started. Most of all, we would like to thank Carl-Johan Helgesson and Mikael Nyström of Ascom for their supervision and input.

Göteborg, June 12, 2014

JONATAN O. ERIKSSON, L. HAMPUS TENGFJORD

Nomenclature

IPS Indoor Positioning System

GPS Global Positioning System

IN Inertial Navigation

INS Inertial Navigation System

DR Dead Reckoning

GNSS Global Navigation Satellite System

RFID Radio Frequency Identification

UWB Ultra-Wide Band

SHS Step-and-Heading System

MEMS Microelectromechanical System

EKF Extended Kalman Filter

G-N Gauss-Newton

CONTENTS

1	INTRODUCTION	1
1.1	Background	2
1.2	Purpose	3
1.3	Scope	3
2	Introduction to the Research Areas and Relevant Work of Others	4
2.1	Wireless Indoor Positioning Systems	4
2.2	Pedestrian Dead Reckoning	5
3	THEORY	8
3.1	Pedestrian Dead Reckoning	8
3.2	Gyroscopes	11
3.3	Accelerometers	12
3.4	Magnetometers	12
3.5	Kinematics	14
3.6	Extended Kalman Filter	18
3.7	Gauss-Newton	19
3.8	Mapping	20
4	Modeling and Implementation	22
4.1	PDR Model	22
4.2	Hardware and Software	25
4.3	Calibration	25
4.4	Kalman Filter	27
4.5	Gauss-Newton	30
4.6	Complementary Filter	33

4.7	Outlier Detection	34
4.8	Mapping	34
5	RESULTS	38
5.1	Orientation Estimation	38
5.2	Magnetometer Evaluation	40
5.3	Step Detection and Length Estimation	43
5.4	PDR System	43
5.5	Mapping	44
6	DISCUSSION	47
	Bibliography	49

1 INTRODUCTION

Due to the ever-growing capabilities of today's mobile devices, those of the *Smart Phones* in particular, and to their abundance, the market for *Indoor Positioning Systems* (IPSs) is expanding, (Harle 2013). An IPS estimates the position of objects, devices, or persons inside buildings. Applications for IPSs can be found in security critical environments such as prisons or hospitals - when an employee sounds the alarm, help can quickly be sent. Fire fighters can be guided inside burning buildings to victims in need of rescue, (Stella *et al.* 2012). They can also be used to monitor and log the movements of personnel, goods, or AGVs to optimize resource utilization, (Lu *et al.* 2013). Other applications are in the retail sector, a well-organized customer, for example, can make a shopping-list before going shopping and then be guided to the items by an application using information about his position as he roams about in the store. He can also be given tailor-made information about special offers on items as he walks past them, (Kopytoff 2013). An elderly nursery home resident at large can, if wearing a device communicating with an IPS, be tracked and subsequently returned back to safety and confinement yet again.

For a long time, tracking technologies have existed. Among the most well-known are the *Global Positioning Systems* (GPSs). Inside indoor spaces, however, many signals, such as those used by GPSs, are prone to be blocked or distorted, rendering such technologies impracticable indoors. The accuracy requirements of IPSs are also often higher than those of their outdoor counterparts. Technologies already deployed often rely on wireless short range beacons, bluetooth or wifi beacons for example, which can substitute GPSs indoors, (Liu *et al.* 2007). They are called *wireless IPSs*. It can, however, be costly to deploy a great number of beacons. To reduce that number, and to enable positioning where the beacons are few and far between, *Inertial Navigation* (IN) can be used. *Inertial Navigation Systems* (INSs) require motion sensors such as accelerometers, magnetometers, and gyroscopes to produce estimates of changes in position. A combination of these two techniques forms a hybrid IPS (Harle 2013).

The accuracy can be further improved if the information given by the INSs and wireless IPSs is combined with knowledge about the physical surroundings, that is, map information. This process is called *mapping*. An array of different mapping techniques exists, most of them compare the estimated trajectory against physically possible trajectories, that is, ones that do not transgress walls or other, most likely, impassable objects, (Attia *et al.* 2013).

A big part of today's research concerning IPSs is focused on the positioning of pedestrians due to their recent inclination toward always carrying Smart Phones with them. These devices come equipped with the motion sensors required by INSs as well as the ability to communicate with a variety of beacons, making them poised to serve as indoor tracking devices, (Lee *et al.* 2002). The process of calculating the trajectory of a pedestrian with data from inertial sensors is called *Pedestrian*

Dead Reckoning (PDR). Magnetometers are also often included in PDR systems. A fundamental part of PDR is to use accelerometers and gyroscopes to measure linear accelerations and angular rates to determine the device's position and orientation, (Kang *et al.* 2012).

The gyroscopes and accelerometers found in Smart Phones and many other mobile devices are cheap as well as microscopical in size. They are so called *MEMS-sensors*, (Jimenez *et al.* 2009). For all their advantages, though, there is one department in which they lack; the quality. The gyroscopes often suffer from both noise and bias. Integrating a noise-ridden and biased signal will inevitably lead to a drift in whatever is estimated. This drift grows large over time and will, if not corrected, lead unacceptable errors in orientation. Accelerometers, too, suffer from these imperfections, and if the measurements they provide were to be integrated twice into a traveled distance, the errors would be vast. To reduce the drift brought on by the signals' noise and bias, the greatest adversaries of Dead Reckoning, it is common to go about the problem in other, not as brute-force, ways.

A PDR system is often divided into two parts, one estimating the length of each step and the other the heading, (Harle 2013). The orientation is often estimated with the use of both the gyroscope and accelerometer data. The perpetual force of gravity is measured by accelerometers, and the measurements give an absolute estimate of a part of the device's orientation, namely the *tilt angles*. Thus part of the gyroscope's drift can be compensated for by an accelerometer. The drift of the remaining part of the orientation, the *heading*, can be reduced measuring the earth's magnetic field or by using mapping. For the step length estimation it is popular to use the vertical acceleration of the device. In order to get it even when the device is tilted, the device's orientation has to be estimated, (Roetenberg 2006).

When carried in the pocket, which is common, phones and other devices are often tilted in various ways. To be able to update the heading no matter how the phone is tilted, its orientation must be estimated, both in relation to the person carrying it, and to the world. One of the main objectives of this project was to intertwine data from different sensors, riddled with noise, into a precise estimate of the orientation. A quaternion-based model was chosen to describe this orientation. The gyroscope and the accelerometer are used to estimate the tilt angles, the gyroscope is also used to estimate changes in the heading. Methods that try to find pure measurements of the earth's magnetic field and subsequently use that data to get absolute measurements of the heading are evaluated. Multiple filters fusing the data from the different sensors are compared. A simple mapping algorithm was devised, implemented, and tested.

1.1 Background

This master's thesis was carried out at the company Ascom in Gothenburg, Sweden. Ascom is a company whose focus is on wireless solutions, on-site communication,

and network testing.

1.2 Purpose

The purpose of this thesis project is to develop a PDR system that estimates changes in position, and that can be used in between updates from overlying wireless IPSs. It should utilize the sensors that modern mobile devices are commonly fitted with and interfere as little as possible with user habits. It should be able to exploit map information to further improve accuracy.

1.3 Scope

The PDR system is to use accelerometers, magnetometers, and gyroscopes. Other sensors which often come in the same package as the aforementioned are pressure sensors and thermometers. The PDR system is limited to only detect changes in position in the horizontal plane, that is, it will not detect if a user walks up a flight of stairs or takes the elevator to another floor. For that reason pressure sensors, which are commonly used to detect changes in altitude, will not be used. Thermometers can be used for calibration purposes, but due to time limitations they have not been utilized. The mobile device is limited to be carried either in the pocket or on the hip.

2 Introduction to the Research Areas and Relevant Work of Others

Indoor Positioning, inertial navigation, and Pedestrian Dead Reckoning have been hot research areas for the past decade or so. Some of the work done in previous research is presented below, divided into sections based on technologies used and where the tracking device is placed on the body.

2.1 Wireless Indoor Positioning Systems

Historically, a majority of the work on IPSs has been based on the same principle as *Global Navigation Satellite Systems* (GNSS), i.e. triangulation. These wireless indoor positioning systems are often based on technologies already commonly deployed, for example WiFi systems. The advantage of using existing technologies is that in many buildings the infrastructure is already there. However, a downside is that the infrastructure is not optimized for position tracking. An infrastructure designed to be used by IPSs can achieve high accuracy though. Different IPSs have different demands on location information. Some need an absolute position, others a relative or a symbolic. A symbolic position can be, for example, which room the device is located in. Depending on the application, the tracking coordinates are expressed in 2-D, a map, 2.5-D, a map with floors, or in 3-D (Liu *et al.* 2007).

Existing wireless IPSs technologies are primarily based on technologies such as GPS, *Radio Frequency Identification* (RFID), WLAN, Bluetooth, *Ultra-Wide Band* (UWB), as well as cellular technologies such as *Global Systems for Mobile Communications* GSM technology. There have been a lot of improvements recently in receiver technologies, which has led to that the performance of wireless IPSs has increased, e.g. UWB systems have reached accuracies down to decimeters. Some problems still exist with these technologies, though, usually related to the environment where they are used, e.g. inside buildings, where multipath noise and other noises exist. Nonetheless, these problems can be circumvented and a high enough accuracy can be acquired for most applications. The main remaining issue with wireless IPSs is the cost to set up the system and its infrastructure, (Harle 2013), (Liu *et al.* 2007). The in-depth details of these technologies, and their problems, are outside the scope of this thesis.

2.2 Pedestrian Dead Reckoning

A branch of IPSs that gains increasingly more attention consists of the PDR systems. They utilize inertial measurements to track the user using various dead reckoning methods. An important aspect of PDR is that it only provides relative position, thus a starting position is most often needed. For this reason PDR systems are usually hybrid systems, employing a position update from a wireless IPS from time to time, from which the PDR system takes over, (Harle 2013).

The inertial sensors PDR systems use are accelerometers and gyroscopes. They can also utilize; magnetometers to estimate the direction toward the magnetic north, pressure sensors to estimate changes in altitude, and thermometers to estimate changes in temperature. The temperature is not used in the position estimation directly but used to model temperature dependent behaviors of the other sensors, (Kouroggi *et al.* 2010), (Fang *et al.* 2005).

The methods used in PDR differ with field, what kind of walking movements are considered, and where the sensors are attached, on a boot, in a backpack, in a pocket, et cetera. They also differ with environment, in a similar fashion wireless IPSs do. In some buildings disturbances in the magnetic field limit the possibility of using magnetometers, thus creating a need for new magnetometer models.

Generally PDR systems rely on one of two different constellation of sensors. The first utilizes inertial sensors together with magnetometers, where the magnetometers give the absolute heading which gives the possibility to correct the gyroscope's bias drift. Also, gyroscopes only give relative heading, whereas magnetometers can provide an initial heading. The other is a more basic approach that makes use of only inertial sensors, with the reasoning that there are too many disturbing magnetic fields indoors, (Foxlin 2005) and (Kwanmuang *et al.* 2011). In both approaches the combination of a 3-axis gyroscope together with a 3-axis accelerometer is standard.

Most PDR systems are designed to work when the user is walking normally, they detect the steps and then estimate the distance with the help of the steps. This means that they do not work as good under other circumstances, for example when the user is crawling or strafing. There are, however, other systems that instead estimate the position with the planar acceleration measurements provided by the accelerometer, (Watanabe and Minegishi 2009). These systems are not as limited with regard to the way the user is moving as the general PDR systems.

The focus here is on so called Step-and-Heading Systems (SHSs). They model the motion of a person as a sequence of steps. Each step has a length and a heading that when combined become a *Step Vector*. The trajectory is then created incrementally by adding each new Step Vector to the previous, (Harle 2013). One common method for detecting the steps is to analyze the measured vertical acceleration. The same measurements are also used to determine the step's length. Another method is to analyze the pendulum motion the sensors are subjected to when they are worn on the leg or the hip. The heading is usually estimated by integrating the gyroscope's

angular rates. A magnetometer has been utilized by (Faulkner 2010) to reduce the drift in the heading angle which stems from the gyroscope's bias and noise.

Some different types of PDR techniques commonly used are detailed below, grouped after where on the body the inertial sensors they rely on are located. Depending on this location, the sensors are subjected to different motions and these can be used in various ways to improve the accuracy of the position estimate. The restrictions on the sensors' size and weight are also somewhat location dependent.

Backpack-Mounted Inertial Navigation

One branch of the PDR systems consists of the Backpack-mounted PDRs. The sensors these systems rely on are the same as those other PDR systems usually rely on; accelerometers, gyroscopes, and magnetometers. They are often of high performance but heavy. Backpack-mounted PDR systems could be relevant in application areas wherein the users are carrying heavy equipment for other reasons. The additional weight of the sensors would not have as large an impact in those cases as it would in other. A backpack strapped hybrid solution using a 1 degree per hour drift gyroscope, and accelerometers, together with a GPS was tested in (Jussi Collin 2003). The performance for a 1-axis, and a 3-axis gyroscope was tested, and it was concluded that a 1-axis gyroscope is sufficient if two requirements are met.

1. The initial angle between the local frame's vertical axis and the sensor frame's vertical axis is known, and
2. No rotation along the local frame's horizontal axes occurs.

The Backpack-mounted PDRs generally produce good results, with only a minor drift in heading over time. However, gyroscopes of equal quality to those used by such systems are generally only found in vehicles because they are not convenient to carry around in most cases, nor are they possible to put inside mobile devices, due to their weight and size, (Jussi Collin 2003).

Boot-Mounted Inertial Navigation

The inertial sensors can also be put on or inside a boot. This is often the case when rescue workers are the ones who are to be tracked. This location has the advantage that it is known that the module is fixed relative to the foot. In addition, there will be intervals during gait where the sensors are not moving. These intervals take place when the foot is on the ground and can be used to estimate the sensors' bias (Castaneda and Lamy-Perbal 2010). A more refined gait model to estimate bias drift was proposed by (Suh and Park 2009). Their model effectively increased the heading accuracy. However, it was only tested on 14 meter long intervals so it can

not be completely concluded that their sophisticated gait model increases the overall tracking performance.

Pocket Placed Inertial Navigation

A majority of people have their phone placed in the trouser pocket, it is particularly common among young males, (Ichikawa *et al.* 2005). These phones often have built-in inertial sensors. Because of that, much of the research focuses on how PDR systems work under these conditions. The device is subjected to more or less the same motions when worn on the hip as when placed in the pocket. In (Judd and Vu 2008), they evaluated how their PDR system worked when the device was put in different places on and around the hip. They found that mounting the module on the front or the back of the torso produced the best results, whereas accuracy is reduced when it is attached to the side of the hip. Their method is based on the assumption that the module is fixed with respect to the body. However, if this assumption does not hold and the phone's orientation relative to the body changes, the model could faultily interpret that as a change in heading. Thus, their approach is somewhat unrealistic when it comes to normal Smart Phone usage. The assumption that the phone is fixed relative the body does generally not hold when it is worn in a pocket.

Allowing for a non-fixed position in the pocket opens up for a new problem, that the device's orientation is not fixed with respect to the body. Methods that make use of the placement of the device by analyzing the swing motion during gait are proposed in (Bissig *et al.* 2013), and (Steinhoff and Schiele 2010). They use the gyroscope together with the accelerometer to determine the orientation angles of the phone. The start and the end of the step are estimated using the extrema in the orientation. The orientation transition provides the length of each step. This method is allegedly better at detecting low frequency steps compared to methods using the accelerometer as a pedometer.

A novel approach where a more relaxed view on where the phone is located on the body was made in (Blanke and Schiele 2008), and (Kunze *et al.* 2005). They tried to detect the phone's position on the body and act accordingly, with relatively good results.

3 THEORY

The inner workings of PDR are described in detail in the following section. To be able to convert measurements from the built-in sensors of today’s mobile devices to changes in position, some knowledge of kinematics, sensor theory, and filtering theory is required. The angular rates taken from a gyroscope, for example, can be used to detect changes in the walking direction, no matter how the device is borne by a person. The mathematics allowing for such conversions is one of the topics that will be touched upon in the following section. Furthermore, methods for the fusing of different sources of information are described.

3.1 Pedestrian Dead Reckoning

When modeled, a person’s movement can be divided into three parts, the first determining when steps occur, the second the steps’ lengths, and the third the person’s heading each step. The step detection and the step length estimation are often strongly connected. As mentioned before, PDR systems are often Step-and-Heading systems. The three steps a SHS takes are:

1. Detect when a step occurs
2. Estimate its length
3. Estimate its heading

In a coordinate frame where the x-axis points toward north, the y-axis east, and the z-axis toward the Earth’s core, the motion of a person can be mathematically described by

$$x_{k+1} = x_k + L_k \sin(\psi_k) \tag{3.1}$$

$$y_{k+1} = y_k + L_k \cos(\psi_k) \tag{3.2}$$

where ψ is the heading angle and L the step length. The system has to be provided with initial values for x and y , that is, it has to be provided with a starting position.

In most PDR systems the heading estimate is the major source of error in position, the exception being when the user moves about in an extraordinary style, for example when crawling or strafing. (Harle 2013). Moreover, if the system is to work when the device is tilted, this tilt has to be estimated and compensated for. The tilt angles can be estimated by fusing angular rates from the gyro with measurements of the gravitational force from the accelerometer (Madgwick *et al.* 2010).

Step Detection

It is common to use the accelerometer’s signal to detect steps, but the signal has different characteristics depending on where the device is placed on the body. The focus here has been on methods that work when the device is placed on the hip, in the leg pocket, or in the breast pocket. If the device is placed on the boot, the accelerometer signal do not exhibit the characteristics these models require to work optimally (Godha and Lachapelle 2008).

The measured vertical acceleration can be used to detect when steps occur, a model that does so is the one proposed by (Weinberg 2002), which uses a single axis accelerometer. There are two key accelerations that act on the device during each step. The first happens at the beginning of the step when the leg the pushes the body upwards which leads to a large negative vertical acceleration. The second takes place when the leg swings back and the body moves forward which leads to a large positive vertical acceleration. These values can also be used to estimate the length of the steps, assuming that the acceleration increases with longer steps. A plot of the estimated vertical acceleration of a device carried in the pocket is shown in Figure 3.1.

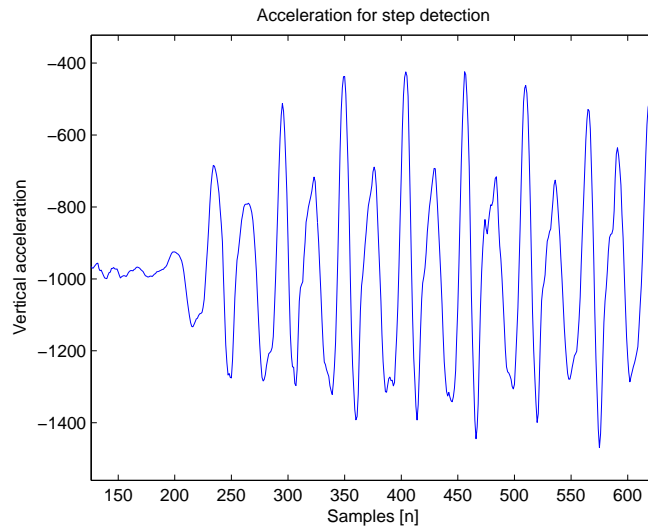


Figure 3.1. The accelerometer signal during some steps.

For cases when the sensors are located in a pocket, on the leg, or on a shoe, the device’s orientation can be used for step detection. (Steinhoff and Schiele 2010), (Bissig *et al.* 2013). These methods are based on that the orientation of the leg changes periodically during walk. They derive and use the equations

$$\mathbf{L} = L_C \cdot \mathbf{L} + (1 - L_C) \cdot \mathbf{g} \quad (3.3)$$

$$\mathbf{r} = \mathbf{g} \times \mathbf{L} \quad (3.4)$$

$$\mathbf{H} = H_C \cdot \mathbf{H} + (1 - H_C) \cdot \mathbf{r} \quad (3.5)$$

$$\Phi = \arccos((\mathbf{L} \times \mathbf{H}) \cdot \mathbf{g}) \quad (3.6)$$

in which \mathbf{L} is the vector aligned with the leg, \mathbf{H} is the vector pointing away from the hip, \mathbf{g} the gravitational vector expressed in the Sensor Frame, and \mathbf{r} is the rotation axis vector. The vectors \mathbf{L} and \mathbf{H} are low-pass filtered with the constants L_C and H_C . The angle Φ is the inclination angle between the \mathbf{g} and $\mathbf{L} \times \mathbf{H}$. An illustration of the vectors and Φ is shown in Figure 3.2. The maxima and minima of Φ can then be used to detect when steps occur.

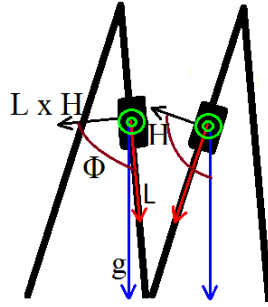


Figure 3.2. Depiction of the vectors \mathbf{L} , \mathbf{H} , \mathbf{g} , and \mathbf{r} at the two extrema of a step.

Step Length Estimation

The step length could be estimated by integrating the horizontal acceleration twice over each step. Doing so with noisy data would bring on vast errors. Instead the information from the step detection models described above can be used to estimate the steps' length.

The equation

$$L = K(\max(acc) - \min(acc))^{1/4} \quad (3.7)$$

has been used by many, and was first proposed by (Weinberg 2002). In Eq. 3.7 K is a constant which has to be tuned for each person. This model is based on the assumption that the difference between these two extrema increases with longer steps.

The model that (Bissig *et al.* 2013) proposed calculates the angle between the two opposite extrema of the leg orientation and uses it to estimate the step length. This

angle, denoted as α , is the difference between the two extrema of the angle Φ in Eq. 3.6

$$\alpha = \Phi_{max} - \Phi_{min}. \quad (3.8)$$

The step length, L , is then calculated as

$$L = c \sin \frac{\alpha}{2} \quad (3.9)$$

where c is constant tuned for the individual tracked.

Step Heading

There are many ways of estimating the step heading, many make use of gyroscopes while others use magnetometers or a combination of the two. Changes in the heading angle can be estimated by integrating angular rates from gyroscopes. This can be done in numerous ways, some of them will be described later. The heading can be calculated from the ratio between measurements of the Earth's magnetic force in two perpendicular directions that lie in the horizontal plane. These are denoted as h_x and h_y , respectively. The equation

$$\Psi = \arctan \left(\frac{-h_y}{h_x} \right). \quad (3.10)$$

is then used to calculate the heading. If x points toward the magnetic north and y toward the magnetic east, then the estimated heading should be zero.

The problem with the approach using the gyroscope is that its long term accuracy is poor due to the noise and bias that exist on the gyroscope's signal. The other approach, using the magnetometer, does not suffer from the same drift but is instead very noisy. On top of that, indoors there are many disturbing magnetic fields which come from electronic equipment as well as ferromagnetic materials, (Kwanmuang *et al.* 2011). One way to reduce the drift in the first approach is to estimate the bias of the gyroscope. That was done by (Madgwick *et al.* 2010).

Both approaches can be used in conjunction, and if successfully done so, the imperfections of each of sensors can be compensated for by the other. This has been done by many, for example by (Marins *et al.* 2001).

3.2 Gyroscopes

A gyroscope is a sensor that can be used to measure angular rates. A wide range of gyroscopes exists, some are simple mechanical devices while others rely on far more advanced technologies, such as the quantum gyroscopes. Their sensitivity ranges from the coarse precision of the MEMS-gyroscopes to the stellar accuracy of the quantum gyroscopes. The gyroscopes found in Smart Phones and other mobile

devices are based on MEMS-technology, and have thus limited precision. These gyroscopes are affected by temperature, and will for that reason have to be recalibrated from time to time to maintain even a modest precision (Jay Esfandyari 2010).

3.3 Accelerometers

Unable to transgress nature's laws, accelerometers measure not only actual changes in velocity but also the force that gravity inexorably exerts on them. They are said to measure the proper acceleration. The proper acceleration is the acceleration relative to a free-fall observer whose acceleration is g toward the core of the earth. Many modern mobile devices come equipped with 3-axis accelerometers, each of their axes are perpendicular to the others. If one of the axes of an accelerometer moving with constant velocity points directly toward the earth's core, it should measure an acceleration of $-g$ while the other two should measure no acceleration. This can be exploited to get an absolute measurement of the device's tilt angles (Pedley 2013).

3.4 Magnetometers

A magnetometer is an instrument that measures magnetic fields. It can measure the magnetization of a magnetic material, the Earth's magnetic strength in a specific direction, or the direction of the earth's magnetic field. In a lot of new devices magnetometers are included, high and medium end Smart Phones and GPS receivers, for example, often have 3-axis magnetometers, and cars often have 2- or 3-axis magnetometers. These magnetometers are commonly used as *electronic compasses* (eCompass) (Pedley 2013).

First, some basic theory on the earth's magnetic field and how to determine the direction of the true magnetic north, for a certain location on Earth three pieces of information are needed.

1. The declination angle. The angle between the magnetic north and the true north.
2. The inclination angle. The angle between the Earth's horizontal plane and the Earth's magnetic field lines.
3. The strength of the magnetic field.

The inclination angle naturally varies between -90° in the south hemisphere to $+90^\circ$ in the north. The magnetic field strength ranges from 25 to 65 $\mu Tesla$ based on location and it also varies over time. When it comes to navigation the declination

angle is of special interest, and over time it has undergone a lot of changes. Local differences affecting these three variables are due to the variations in the Earth's core, and the composition of the ground, a high composition of iron ore, for example, interferes with the magnetic field. There are also significant time-variant changes, where the declination angle changes up to 0.4° a day. Changes in time are due to magnetic storms in short terms, and secular variation that has variations on a big time scale ranging from milliseconds to millions of years. Secular changes reflect changes in the Earth's core, (*Magnetic declination* 2014) and (Gauss 2014). As of the date 2014-03-20, in the Gothenburg region, the declination and the inclination angles were, $2^\circ 47' 37''$ and $71^\circ 23' 59''$ respectively. The magnetic field strength was 50,653.4 nT, (NOAA 2014).

The Earth's geographic coordinate system is defined as a perpendicular x-y-z system, the x-axis pointing north, the y-axis pointing east, and the z-axis pointing down. To estimate the direction of the magnetic north two magnetometers are needed. A common setup is to have the two sensors representing the Earth's x-axis and the y-axis respectively. The heading is defined as clockwise rotation along the Earth's z-axis. In the Earth's horizontal plane a magnetic component is only detected toward the magnetic north, along the west-east axis no magnetic field is seen, and with given magnetometer readings the heading is

$$\text{Heading} = \text{atan2}\left(\frac{-m_y}{m_x}\right) \quad (3.11)$$

The function `atan2` gives a full coverage of the range $[-\pi, \pi]$. The heading must then be adjusted for the declination angle.

As with all sensors, magnetometers accuracies range over a wide spectrum, where *microelectromechanical systems* (MEMS) sensors are found in the very low regions. Due to the low accuracy of these MEMS magnetometers there is no point in being overly anal about a perfect adjustment of the declination angle for these sensors. It is more critical to calibrate the sensors with respect to gain and bias than it is to find a good estimate of the declination angle. Because the sensors are located where they are, on a chip, magnetic interference from that chip is present. Thus a big part of the offset is due to this interference, (ST 2010). By knowing the magnetic field strength of the Earth, the chip's magnetic field can be compensated for.

Outlier Detection

When ambulating indoors, the magnetometer measures constantly changing magnetic fields. It is, however, the Earth's magnetic field it needs to measure if it is to give an absolute estimate of the device's and the person's heading. Therefore, if the magnetometer is to be used to that end, an outlier detector, that discriminate the pure readings of the Earth's magnetic field from the disturbed, has to be used.

The detector used by (Lee and Park 2009) calculates the difference between the magnitude of the magnetometer's measurement vector and a reference magnitude,

which often is the Earth's magnetic field vector. If this difference is larger than a certain threshold, the magnetometer is not used to update the orientation estimate. Mathematically this condition can be put as

$$||m_M| - |\mathbf{h}|| < \epsilon_M \quad (3.12)$$

where m_M is the measurement vector, \mathbf{h} the Earth's magnetic field vector, and ϵ_M the threshold.

In the system proposed by (Sabatini 2006) the ratio between the magnitude of the horizontal components and the total magnitude of the measured magnetic fields is used. They call this ratio the *Dip Angle*. They calculate it as

$$\alpha = \arccos \left(\frac{\sqrt{m_{M,x}^2 + m_{M,y}^2}}{|m_M|} \right) \quad (3.13)$$

where α is the Dip Angle. The Dip Angle is then compared to a location dependent reference angle

$$|\alpha - \alpha_{ref}| < \epsilon_{dip}. \quad (3.14)$$

According to (Callmer *et al.* 2013) no one of the two outlier detection conditions above succeeds in singling out the good measurements. In their stead, they propose that the difference in angular rates from the gyroscope and magnetometer should be looked at. They calculate this difference, λ , as

$$\lambda_k = y_k^h - y_{k-1}^h - T y_{k-1}^\omega \quad (3.15)$$

where y^h is the heading according to the magnetometer, T the sampling time, and $T y^\omega$ the change in heading according to the gyroscope. This λ can sometimes be small even though the magnetometer is disturbed, just by coincidence. To reduce the impact of such coincidences, the average of λ over a number of samples,

$$\bar{\lambda}_k = \frac{1}{N} \sum_{i=k-N+1}^k |\lambda_i| \quad (3.16)$$

is used to determine how disturbed the reading is instead.

3.5 Kinematics

If an object is to be tracked in a three-dimensional frame, it is reasonable to describe its motion with a mathematical model that considers three dimensions as well. The mathematics describing the motion of a rigid body, be it linear or angular, is called *Kinematics*. Linear motion and acceleration can be described the same way in three dimensions as in two, they can be decomposed into components along arbitrary axes with simple trigonometry. The same does not quite go for rotations in three

dimensions. It is, however, key to correctly handle rotations in $\mathcal{3}$ -space when the angular rates from the gyroscope, measured in the device's frame, are to be used to update the heading of the device, and of the person carrying it. For that reason, a summary of the workings of 3-space rotations will be given below.

Rotations in 3-space

A rotation, whether two- or three-dimensional, can either be point- or frame-fixed. The former is a rotation of the coordinate frame with respect to a fixed point, or a vector, the latter the rotation of a point, or a vector, with respect to a fixed frame (Kuipers 1999, p. 47). Both types can be expressed mathematically with so called rotation matrices. A rotation matrix either maps a point from one coordinate frame to another, or rotates a point within a frame. Mathematically such a coordinate transformation can be put as

$$p^\omega = R^{b/\omega} p^b$$

where $R^{b/\omega}$ is the matrix and p^ω and p^b are the point coordinates expressed in their respective frames.

It so happens that the rotation matrix pertaining to a frame-fixed rotation is the inverse, and transpose, of the corresponding point-fixed rotation.

$$R^{-1} = R^T$$

and

$$R^{b/\omega} = R^{\omega/b^T}$$

(Kuipers 1999, p. 53).

In order to use the device's measurements, given in the body frame, to track its position in the world frame, the relationship between those two frames has to be known, or estimated.

Euler Angles

The device's orientation is defined, here, as the device's angular position in relation to the world frame. It can be described by three subsequent rotations about a certain set of axes. These align the world frame's axes with the device's. The angles related to those rotations are called the Euler Angles. In this thesis the axes rotated round are those of the rotating coordinate system, namely the body axes. The same body axis can be rotated round twice, but not back to back. For example; XYX is a valid sequence whereas XXY is not. There are 36 different sequences in total, (Kuipers 1999, p. 52).

The definition used in this project of the world frame's axes is; the x-axis points toward the north, the y-axis east, and the z-axis toward the earth's core. This

definition agrees with the so called right hand rule. The rotation sequence used is the so called *Aerospace Sequence* in which the sequence of rotation axes is ZYX, where the final total rotation matrix is calculated as

$$T = T_\phi T_\theta T_\psi = \begin{bmatrix} 1 & 0 & 0 \\ 0 & \cos \phi & \sin \phi \\ 0 & -\sin \phi & \cos \phi \end{bmatrix} \begin{bmatrix} \cos \theta & 0 & -\sin \theta \\ 0 & 1 & 0 \\ \sin \theta & 0 & \cos \theta \end{bmatrix} \begin{bmatrix} \cos \psi & \sin \psi & 0 \\ -\sin \psi & \cos \psi & 0 \\ 0 & 0 & 1 \end{bmatrix} \quad (3.17)$$

The three angles, Ψ , θ , and ϕ , of the Aerospace Sequence are called heading, elevation, and bank, respectively. The heading is the rotation about the Z-axis of the world, the elevation the angle about the intermediate Y-axis, and the bank the rotation about the device's final X-axis. A depiction of an example Aerospace Sequence is shown in Figure 3.3.

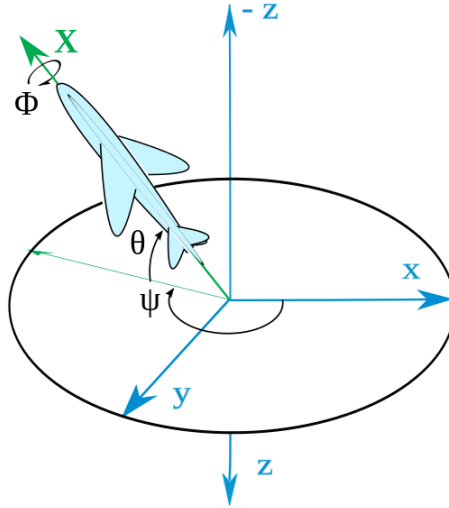


Figure 3.3. The Aerospace Euler Angles, heading ψ , elevation θ , and bank ϕ

Given a rotation matrix, the measurements from both the accelerometer and magnetometer can be easily converted from one of the frames to the other, since they are linear quantities. Converting angular rates from one frame to another is not as straightforward. A substantial amount of algebra has to be done to arrive at the equation

$$\begin{bmatrix} \dot{\phi} \\ \dot{\theta} \\ \dot{\psi} \end{bmatrix} = \begin{bmatrix} 1 & \sin \phi \tan \theta & \cos \phi \tan \theta \\ 0 & \cos \phi & -\sin \phi \\ 0 & \sin \phi \sec \theta & \cos \phi \sec \theta \end{bmatrix} \begin{bmatrix} \omega_x \\ \omega_y \\ \omega_z \end{bmatrix} \quad (3.18)$$

which can be used to update the Euler Angles given angular rate measurements in the body frame (Kuipers 1999, p. 259). It is easy to notice that there exist

singularities in Eq. 3.18 at $\theta = \pm\frac{\pi}{2}$. These stem from a phenomenon called a Gimbal Lock which essentially causes the loss of one degree of freedom.

Quaternions

The existence of singularities among the Euler Angles is one drawback. Another is that concatenating rotations is both unintuitive and computationally expensive. For those reasons, Euler Angles are unfit to represent the orientation in applications wherein incremental angular updates of constantly changing frames are present. In their stead, quaternions, or rather unit quaternions, can be used. The Quaternions can be viewed as extensions of the complex numbers into 3-space. A complex number has a one-dimensional imaginary part, whereas a quaternion has a three-dimensional. A quaternion is often written as

$$q = [q_0, q_1, q_2, q_3]^T \quad (3.19)$$

where the first element, q_0 represents an angle and the other three a vector. It is a so called angle - axis representation. Given an angle α and axis \mathbf{v} the corresponding quaternion is given by

$$q = \begin{bmatrix} \cos(\alpha/2) \\ \sin(\alpha/2)\mathbf{v} \end{bmatrix} \quad (3.20)$$

Compared to Euler Angles they are computationally sounder in the sense that it is easier to keep a quaternion normalized than maintaining orthonormality when updating a rotation matrix with many small rotational perturbations. Like Euler Angles, a quaternion can easily be converted into a rotation matrix with the formula

$$T(q) = \begin{bmatrix} 2(q_0^2 + q_1^2) - 1 & 2(q_1q_2 - q_0q_3) & 2(q_1q_3 + q_0q_2) \\ 2(q_1q_2 + q_0q_3) & 2(q_0^2 + q_2^2) - 1 & 2(q_2q_3 - q_0q_1) \\ 2(q_1q_3 - q_0q_2) & 2(q_2q_3 + q_0q_1) & 2(q_0^2 + q_3^2) - 1 \end{bmatrix}$$

(Kuipers 1999, p. 126).

Concatenating rotations expressed in an ever-changing frame is simple with quaternions. The quaternion related to the incremental rotation, $\bar{\omega}$, is calculated with Eq. 3.20 and is then right hand *quaternion multiplied* with the quaternion describing the previous orientation

$$q_{k+1} = q_k \otimes \bar{\omega}. \quad (3.21)$$

This means that gyroscope measurements can be used easily to update a device's orientation. There exists an even simpler form yet, when the incremental angles are small

$$q_{k+1} = q_k + T\dot{q}_k = q_k + \frac{T}{2}\Omega(\boldsymbol{\omega}_k) \quad (3.22)$$

where

$$\Omega(\boldsymbol{\omega}) = \begin{bmatrix} 0 & -\omega_x & -\omega_y & -\omega_z \\ \omega_x & 0 & \omega_z & -\omega_y \\ \omega_y & -\omega_z & 0 & \omega_x \\ \omega_z & \omega_y & -\omega_x & 0 \end{bmatrix} \quad (3.23)$$

(Kuipers 1999, p. 264).

3.6 Extended Kalman Filter

In PDR it is common to combine data from different sensors in filters. This process is often called *Sensor Fusion*. The orientation of the device is commonly estimated using Sensor Fusion of the gyroscope, accelerometer, and magnetometer in various constellations. The orientation consists of the device's tilt and heading angles, but does not describe its position.

If the noise-characteristics of the sensors used are known, or closely estimated, the Kalman Filter is often a candidate worthy of consideration. The filter most frequently used in PDR systems is the *Extended Kalman Filter* (EKF). This filter allows for nonlinear models. The nonlinear system is modeled as a number of states with corresponding difference equations, and an observation model

$$\mathbf{x}_k = f(\mathbf{x}_{k-1}, \mathbf{u}_{k-1}) + \mathbf{w}_{k-1} \quad (3.24)$$

$$\mathbf{z}_k = h(\mathbf{x}_k) + \mathbf{v}_k \quad (3.25)$$

where \mathbf{w}_k and \mathbf{v}_k are process and measurement noise, respectively. Both are uncorrelated zero-mean white noises with known covariances. Their covariance matrices are denoted here as Q_k and R_k . The state vector could for example consist of a quaternion, then the prediction in Eq. 3.24 is done using Eq. 3.22. The observation of the state, the orientation, can be done by measuring the force of gravity with the accelerometer and the Earth's magnetic field with the magnetometer, (Kim and Golnaraghi 2004).

The filter algorithm is divided into two steps, the prediction and measurement update step, which estimate the new mean value and variance of the state variable's distribution, $N(\hat{x}, P)$. The prediction step consists of the following equations

$$\hat{x}_{k|k-1} = f(\hat{x}_{k-1|k-1}, u_{k-1}) \quad (3.26)$$

$$P_{k|k-1} = F_{k-1}P_{k-1|k-1}F_{k-1}^T + Q_{k-1} \quad (3.27)$$

and the update of

$$\tilde{y}_k = z_k - h(\hat{x}_{k|k-1}) \quad (3.28)$$

$$K_k = P_{k|k-1} H_k^T (H_k P_{k|k-1} H_k^T + R_k)^{-1} \quad (3.29)$$

$$\hat{x}_{k|k} = \hat{x}_{k|k-1} + K_k \tilde{y}_k \quad (3.30)$$

$$P_{k|k} = (1 - K_k H_k) P_{k|k-1} \quad (3.31)$$

where F_k and H_k are the Jacobians of f and h , and higher order terms are neglected

$$F = J_f = \left. \frac{\partial f}{\partial x} \right|_{\hat{x}_{k-1|k-1}, u_{k-1}} \quad (3.32)$$

$$H = J_h = \left. \frac{\partial h}{\partial x} \right|_{\hat{x}_{k|k-1}}. \quad (3.33)$$

The matrix P is the states' estimated covariance matrix, (Terejanu 2003).

3.7 Gauss-Newton

If the orientation is represented by quaternions, the filter measurement update can be simplified by utilizing a *Gauss-Newton* (G-N) algorithm to find the quaternion that best fit the measurements of the Earth's magnetic field and the force of gravity. Then the measurement update becomes linear, (Lee and Park 2009).

The G-N algorithm is a method for solving non-linear least squares problems, proposed by (Gauss 1857). Compared to the well-known Newton method the second derivative is not needed, which makes it simpler to derive, and possibly less computationally expensive. The objective function to minimize is

$$Q(\mathbf{x}) = \frac{1}{2} \sum_{i=1}^n (y_i - f_i(\mathbf{x}))^2 \equiv \frac{1}{2} \sum_{i=1}^n (r_i(\mathbf{x}))^2$$

in which the number of functions must be greater than the number of variables, $n \geq m$, where m is the dimension of the state vector, $\mathbf{x} \in \mathbb{R}^m$, (Wang 2012).

The method is initialized with a guess, \mathbf{x}_0 , of the states. The variables that minimize the objective function can be estimated iteratively. If a local minimum is found the gradient of the objective functions is zero,

$$\Delta Q(x^*) = \Delta r(x^*)^T \Delta r(x^*) = 0 \quad (3.34)$$

(Wang 2012).

The iterative process to find such a solution can be summarized with the following steps

1. Calculate the Jacobian matrix

$$(J_r)_{ij} = \frac{\partial r_i(x^a)}{\partial x_j} \quad (3.35)$$

2. Calculate the direction toward the minimum of the function

$$\Delta x^a = (J_r^T J_r)^{-1} J_r^T r(x^a) \quad (3.36)$$

3. Take a step toward the minimum

$$x^{a+1} = x^a - \Delta x^a \quad (3.37)$$

4. Repeat until convergence

(Wang 2012).

3.8 Mapping

In this context *mapping* is the process of combining output from PDR systems or similar information with knowledge about the surroundings in which the IPS is operating. It could be knowledge about the position of walls, corridors, or rooms. With that information, many erroneous trajectories can be ruled out. A typical mapping algorithm used together with an IPS checks certain conditions each step. One such condition can be that no wall is between the start and the end position of the step. That a person should walk through a wall - or some other, for humans, impassable object - is, at the very least, improbable. If the INS does, however, claim that such a transgression has taken place, corrective measures can be imposed upon the heading angle as well as the position.

Numerous mapping algorithms exist, some of them are of the most modest of complexities, others almost arcane, (Davidson *et al.* 2010). A well-designed mapping algorithm can greatly reduce the drift in both heading angle and position, (Attia *et al.* 2013). The system proposed by (Attia *et al.* 2013) consists of a PDR part and a mapping part. For each step they do the following

1. Update the old position with information from the PDR system
2. Give the updated position as input to the mapping algorithm

Their mapping algorithm is based on *point-to-curve matching*. It projects the updated position onto the nearest passageway. Information about these passageways is stored in maps. By always placing the updated position in a passageway, walls and other objects are avoided.

One of the more advanced, and common, ways of utilizing map information is to fuse it with trajectory data in *Particle Filters*. Based on Bayesian principles, they test many different hypotheses and cast away those that do not fulfill certain criteria. They are most apt at handling the presence of physical obstacles (Evennou and Marx 2006).

4 Modeling and Implementation

The entire system developed in this project and all its components are detailed in the following sections, starting with an overview of the system, then proceeding with its in-depth details. The system is composed of two sub-systems, a PDR and a mapping, similar to that proposed by (Attia *et al.* 2013). The PDR sub-system utilizes a 3-axis gyroscope, a 3-axis accelerometer, and a 3-axis magnetometer. The tracking device is assumed to be placed in the leg pocket, the breast pocket, or on the hip.

4.1 PDR Model

The PDR-model detailed here is based on a sequence of step-vectors that describe the position of a pedestrian over time. These vectors are assumed to lie in the horizontal plane. The norm and direction of each vector is the corresponding step's length and heading, respectively. The Equations 3.1 and 3.2 are used to describe the position mathematically, and are repeated here for convenience,

$$x_{k+1} = x_k + L_k \sin(\psi_k) \tag{4.1}$$

$$y_{k+1} = y_k + L_k \cos(\psi_k). \tag{4.2}$$

A step length estimation model similar to (Weinberg 2002) was chosen because of its simplicity and relatively good performance. This model requires the vertical acceleration of the person whose steps are to be estimated. In order to attain the vertical acceleration of a device whose vertical axis is not perfectly parallel to that of the navigation frame, its tilt angles must be known. The orientation, which contains the tilt angles as well as the heading, can be approximated by fusing accelerometer, magnetometer, and gyroscope measurements. This can be done in numerous ways, three of them have been implemented in this project.

The heading and tilt angles are extracted from the orientation quaternion provided by each filter. The tilt angles are used in the step length estimation which is then combined with the heading of each step to produce the trajectory.

The PDR model is split into two separate modules, the orientation estimation and the step estimation. Output from the former module is used as input to the latter. The information from the two is then combined to produce the final trajectory. A block diagram of the PDR system is shown in Figure 4.1.

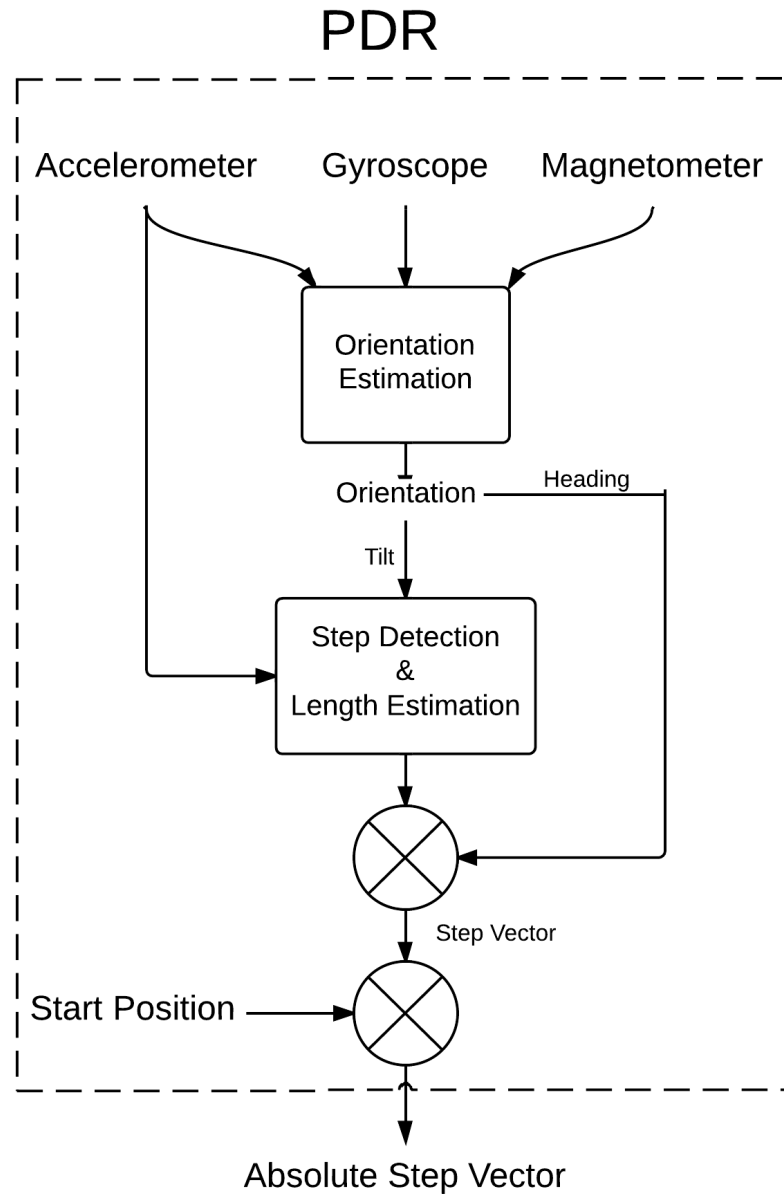


Figure 4.1. An overview of the PDR system.

Orientation Estimation

Three different filters, each one estimates the orientation, have been created. It is much easier to update the orientation with angular rates when it is represented by quaternions than when represented by Euler Angles. That and the Euler Angles' singularities tip the scale in favor of quaternions for the update of the orientation with gyroscope measurements. The equation used to update the orientation with

gyroscope measurements is repeated here for convenience,

$$q_{k+1} = q_k + T\dot{q}_k = q_k + \frac{T}{2}\Omega(\boldsymbol{\omega}_k). \quad (4.3)$$

All three filters use a quaternion-representation for the orientation and exploit the gravitational force to get absolute approximations of the device's tilt and the Earth's magnetic field to get absolute estimates of the device's heading. They differ in how they update their states with accelerometer and magnetometer measurements. The first filter updates the tilt angles separately with Euler Angles and trigonometry in a complementary filter. The second is an EKF that completely operates in the realm of quaternions, unlike the first. The last is also an EKF. It uses a G-N algorithm to find the quaternion that best fits the measured accelerations and magnetic fields to the gravitational acceleration and the Earth's magnetic field, respectively, and this quaternion is then used in the measurement update. The main difference between the first model and the other two is that because they use a quaternion-representation as opposed to an Euler Angle, they are free of singularities. For that reason the latter two models form a sounder base for a PDR.

The way the accelerometer and magnetometer are incorporated into the orientation estimation is different in the three filters, as mentioned before. Their purpose is the same though, to eliminate drift in the orientation.

Step Detection and Step Length Estimation

Since it is the vertical acceleration in the World Frame that is sought, the accelerations measured in the Device Frame have to be transformed. The orientation provided by each of the three filters can be used to create a rotation matrix that is then used to perform this transformation. The equation

$${}^W\mathbf{a} = T(q)^b\mathbf{a} \quad (4.4)$$

describes how such a transformation is done. The vertical acceleration signal is low-pass filtered. The signal is then analyzed, to detect the steps and to estimate their lengths, in a similar fashion as in the model proposed by (Weinberg 2002). The difference is that a 3-axis accelerometer is used instead of a single axis which allows the device to be tilted. To tune the K -value in Eq. 3.7, a known distance is walked and then the K -value is adjusted so that the estimated distance becomes the same as the real. The model was chosen for its relatively high accuracy to complexity ratio. The accuracy of the step length estimation is also less important than that of the heading for the total precision of the position estimation (Chen *et al.* 2010). Figure 4.2 depicts the vertical acceleration during walk with the indices for the beginning and the end of each step as well as the maximum and minimum acceleration during that step marked with crosses and dots, respectively.

The Step Detection and Step Length Estimation can be summarized as

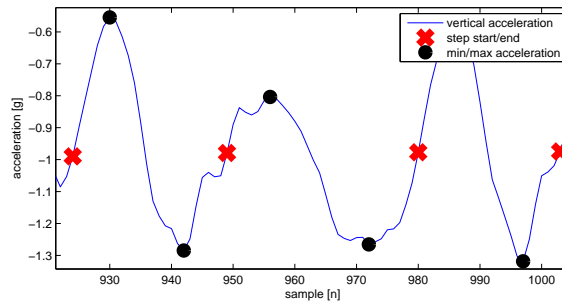


Figure 4.2. The vertical acceleration during normal walk

1. Low pass filter the vertical acceleration signal
2. Find when the signal crosses the gravitational force, $-g$, with a positive slope
3. Find when the next such crossing occurs
4. Find the minimum and maximum values of the signal between these two crossings

Sometimes false crossings occur, these can, however, be detected by asserting that the maximum value is larger than a certain threshold and the minimum smaller than another threshold.

4.2 Hardware and Software

An inertial module, ST's iNEMO-M1, was used. This module has built-in gyroscopes, accelerometers, and magnetometers, each one of them able to take measurements along and about three axes. The module is programmable and can run on-line applications. It can also store sensor data in logs and send data in real-time over wireless networks and USB connections.

The software coming with the iNemo module, iNemo Suite, was used for logging and sending sensor data. The data was processed off-line in MATLAB to test and verify the models. Some of the models were implemented in C++ for real time testing of the orientation estimation.

4.3 Calibration

The inertial unit, iNEMO, used is composed by a 3-axis gyroscope, accelerometer, and magnetometer. There will always be disturbances present on the sensor's measurements for various reasons. These are biases, offsets, and noises. To lessen the effects of these, calibration of the sensors can be performed.

Gyroscope Calibration

The gyro signal ω_G can be modeled as the sum of true angular velocity in the body frame ${}^b\omega$ multiplied by a gain term α_G , a bias term β_G , and measurement noise v_G .

$$\omega_G = {}^b\omega \cdot \alpha_G + \beta_G + v_G$$

The noise term is modeled as zero mean Gaussian noise, and its variance is generally small enough not to pose a problem. The bias term on the other hand will introduce a drift, which limits the accuracy of the orientation estimation and it is thus vital it is corrected. This drift, β_G , can be estimated, and can also be compensated for with other sensors. It is estimated during stationary position, when the real angular rate of the device is zero, simply by taking the mean value of the measurements over a period of time. The gain α_G can be estimated by knowing the real angular velocity. The sensor is rotated around its axis and the measured rotation is compared with the real. It is calculated with

$$\alpha_G = \frac{\omega_G - \beta_G}{{}^b\omega}. \quad (4.5)$$

All three axes are calibrated in the same fashion.

Accelerometer Calibration

The accelerometer signal is modeled similarly to the gyroscope's, with a gain, bias, and noise term. The difference is that not only is the body's motion affecting the signal, the perpetual gravitational acceleration is too.

$$a_A = ({}^b\mathbf{g} + {}^b a_{body}) \alpha_A + \beta_A + v_A \quad (4.6)$$

To estimate β_A , the accelerometer can be aligned perpendicularly to the gravitational field so it is not affected by gravity, but it is difficult to find a perfect alignment. Instead, the parameters α_A and β_A are estimated by aligning the sensor with, and opposite, \mathbf{g} , where the true acceleration is $\pm|\mathbf{g}|$. Thus the min and max values, a_A^{min} and a_A^{max} , are found and used to estimate the gain and bias as

$$\alpha_A = \frac{a_A^{max} - a_A^{min}}{2|\mathbf{g}|} \quad (4.7)$$

and

$$\beta_A = \frac{a_A^{max} + a_A^{min}}{2\alpha_A}. \quad (4.8)$$

Magnetometer Calibration

The magnetometer measurements are prone to be affected by greater relative disturbances compared to the other sensors. This is because a great portion of unwanted magnetic fields are measured beside the Earth's magnetic field, a part of these are from surrounding construction materials and electric devices, and the other part is from the chip it is located on. With this definition of disturbances the measurements can then be modeled to include the following: the Earth's magnetic field vector expressed in the body frame ${}^b\mathbf{h}$, the chip's magnetic field \mathbf{M}_{chip} , other magnetic fields \mathbf{M}_{dist} , bias α_M , offset β_M , and noise v_M . As the chip's magnetic field is relatively constant this is included in β_M giving the expression of the measurement as

$$m_M = ({}^b\mathbf{h} + \mathbf{M}_{dist}) \alpha_M + \beta_M + v_M$$

Bias α_M and offset β_M are estimated in a disturbance free environment, excluding the chip's magnetic field. All three axes are calibrated simultaneously, data is collected where all axes are at least once aligned and opposite aligned with \mathbf{h} . The biases and offsets are then estimated using the min and max value, m_M^{min} and m_M^{max} .

$$\alpha_M = \frac{m_M^{max} - m_M^{min}}{2|\mathbf{h}|} \quad (4.9)$$

$$\beta_M = \frac{m_M^{max} + m_M^{min}}{2\alpha_M} \quad (4.10)$$

\mathbf{M}_{dist} is time variant disturbances and can not be statically calibrated, instead outlier detection is used to detect its presence.

When measuring the Earth's magnetic field with a 3-axis magnetometer, the norm of the measurement vector is ideally equal to $|\mathbf{h}|$. Considering a 3-D space the measurements should form a sphere with its center in the origin and with a radius of $|\mathbf{h}|$. An uncalibrated magnetometer with biases and offsets will form an ellipsoid sphere with an offset, as seen in Figure 4.3. After the calibration the magnetometer measurements better fit with the theoretical sphere, as seen in Figure 4.4.

4.4 Kalman Filter

The accelerometer and the magnetometer each give as output a measurement vector of dimension three, $[x, y, z]$. The acceleration in the Earth frame is the gravitational force vector, $\mathbf{g} = [g_x, g_y, g_z] = [0, 0, -9.81] \text{ m/s}^2$, and the corresponding vector for the magnetic force in the Earth frame is the Earth's magnetic field, $\mathbf{h} = [h_x, h_y, h_z] = [16.4, 0, 47.8] \mu T$.

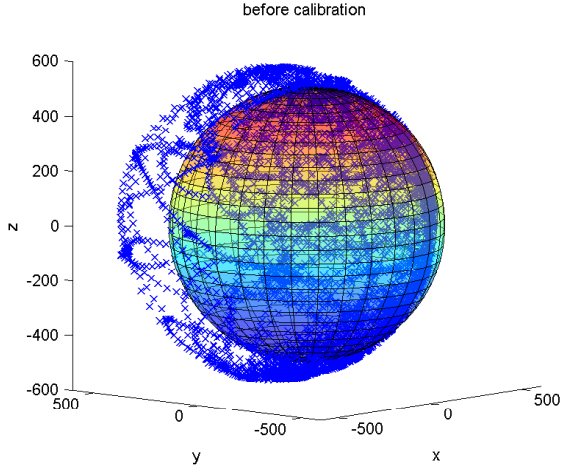


Figure 4.3. Uncalibrated magnetometer

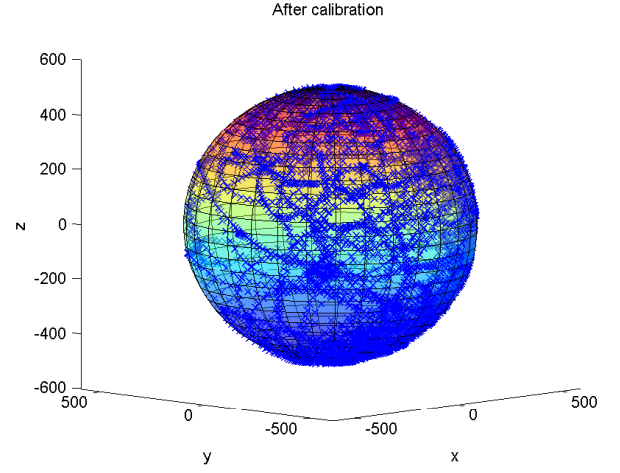


Figure 4.4. Calibrated magnetometer

The states of the EKF are chosen to be the four quaternion components representing the orientation of the device in relation to the World Frame.

$$x = [q_0, q_1, q_2, q_3]^T$$

The angular rates from the gyroscope are taken as inputs.

$$u = [\omega_x, \omega_y, \omega_z]$$

The gyro measurements are after calibration modeled to be the sum of the angular velocity in the body frame ${}^b\omega$ and measurement noise \mathbf{v}_G .

$$\mathbf{u} = {}^b\omega + \mathbf{v}_G$$

Since the accelerometer and the magnetometer provide measurements of the gravitational acceleration and the magnetic field in the body frame it is natural to choose these as outputs of the filter. The sensors do not only give measurements of the gravity and the Earth's magnetic field, although it is only these that are of interest. Outlier detection is used to estimate when the measurements are useful.

The accelerometer measurements after calibration are composed of gravitational force in the body frame ${}^b\mathbf{g}$, the acceleration of the device in the body frame ${}^b\mathbf{a}_{body}$, and measurement noise \mathbf{v}_A . The acceleration, however, is assumed to be zero

$$\mathbf{z}_A = {}^b\mathbf{g} + {}^b\mathbf{a}_{body} + \mathbf{v}_A \approx {}^b\mathbf{g} + \mathbf{v}_A.$$

The magnetometer measurements after calibration include the magnetic field vector in the body frame ${}^b\mathbf{h}$, a disturbance vector ${}^b\mathbf{d}$, and measurement noise \mathbf{v}_M . The magnetometer is assumed to only measure the Earth's magnetic field. The disturbance term, however, is assumed to be zero

$$\mathbf{z}_M = {}^b\mathbf{h} + {}^b\mathbf{d} + \mathbf{v}_M \approx {}^b\mathbf{h} + \mathbf{v}_M.$$

Two separate measurement updates are performed with the measurements from the accelerometer and magnetometer respectively. This because they are subjected to uncorrelated outliers and are therefore not suitable to be used at the same time always.

The process noise covariance matrix was through experiments chosen to be $Q_{gyro} = I_4 \cdot e^{-5}$, and the measurement noise covariance matrices as $R_A = I_3 \cdot e^{-3}$, and $R_M = I_3 \cdot 0.5$.

Prediction Step

The predictions are done using the angular rates, given as inputs, and a sampling time T

$$\begin{aligned} x_{k|k-1} &= f(x_{k-1|k-1}, u_{k-1}) = \\ &= x_{k-1|k-1} + \frac{T}{2} \dot{x}_{k-1|k-1} = \\ &= x_{k-1|k-1} + \frac{T}{2} \Omega(u_{k-1}) x_{k-1|k-1} \end{aligned} \quad (4.11)$$

which leads to the Jacobian matrix

$$F_{k-1} = I_{4 \times 4} + \frac{T}{2} \Omega(u_{k-1}). \quad (4.12)$$

The prediction steps are then performed

$$x_{k|k-1} = F_{k-1} x_{k-1|k-1}, \quad (4.13)$$

$$\mathbf{P}_{k|k-1} = F_{k-1} P_{k-1|k-1} F_{k-1}^T + Q_{k-1}. \quad (4.14)$$

where

$$Q_{k-1} = G_{k-1} Q_{gyro} G_{k-1}^T \quad (4.15)$$

and

$$G_{k-1} = \frac{T}{2} \Omega^*(x_{k-1|k-1}). \quad (4.16)$$

The process noise is obtained from the gyroscope and thus given in terms of angular rates. Equation 4.15 and 4.16 transforms them from angular rate process noise to quaternion process noise. (The Institute of Technology at Linkping University 2013).

Measurement Update Step

The measurement update transforms the gravity vector and the Earth's magnetic field vector from the World Frame to the Body Frame. This is achieved with a

rotation matrix given the current state, $x_{k|k-1}$, multiplied with \mathbf{g} and \mathbf{h} respectively, leading to measurement residuals

$$\tilde{y}_A = z_A - h(x)_A \quad (4.17)$$

and

$$\tilde{y}_M = z_M - h(x)_M \quad (4.18)$$

where

$$h(x)_A = T(x)\mathbf{g} = - \begin{bmatrix} 2(x_1x_3 + x_0x_2) \\ 2(x_2x_3 - x_0x_1) \\ 2(x_0^2 + x_3^2) - 1 \end{bmatrix} |g| \quad (4.19)$$

$$h(x)_M = T(x)\mathbf{h} = \begin{bmatrix} 2(x_0^2 + x_1^2) - 1 & 2(x_1x_3 + x_0x_2) \\ 2(x_1x_2 + x_0x_3) & 2(x_2x_3 - x_0x_1) \\ 2(x_1x_3 - x_0x_2) & 2(x_0^2 + x_3^2) - 1 \end{bmatrix} \begin{bmatrix} h_x \\ h_z \end{bmatrix} \quad (4.20)$$

which are then used to get the Jacobian matrices H_A and H_M .

4.5 Gauss-Newton

If an orientation quaternion were to be given as a measurement from the magnetometer and accelerometer data, the measurement update in the EKF filter could be simplified significantly. The G-N iteration algorithm can be used to find a quaternion that fits the accelerometer and the magnetometer measurement vectors to the known gravitational vector \mathbf{g} and the Earth's magnetic field vector \mathbf{h} , respectively. Such an approach was proposed by (Lee and Park 2009) and (Marins *et al.* 2001). They also state that the gain in computational efficiency from the simplified measurement update outweighs the cost of the G-N step.

The third and last filter is, like the second, a Kalman Filter. The difference is that its measurement update is performed with a quaternion instead of an acceleration vector. The prediction step of the Kalman filter is the same as in the EKF. The prediction is then corrected with the quaternion given by the G-N iteration if the outlier criteria are fulfilled. A filter diagram of the setup is presented in Figure 4.5.

Measurement vectors

The cost function to be minimized is the difference between the known gravitational and magnetic field vectors in the World Frame and to the World Frame transformed

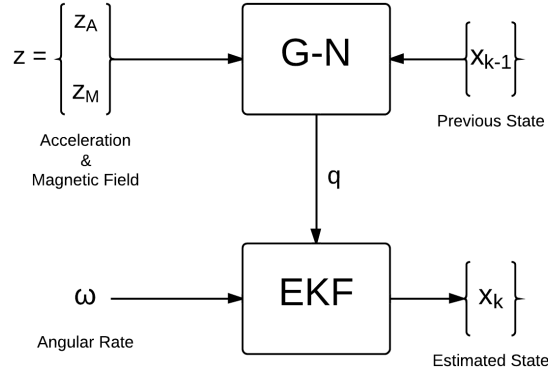


Figure 4.5. The G-N filter diagram.

sensor measurements. The equations

$$C(q) = \frac{1}{2} \epsilon(q)^T \epsilon(q) \quad (4.21)$$

and

$$\epsilon(q) = \begin{bmatrix} \mathbf{g} - Q(q) \cdot \mathbf{y}_{acc} \\ \rho(\mathbf{h} - Q(q) \cdot \mathbf{y}_{mag}) \end{bmatrix} \quad (4.22)$$

express the cost function, where ρ is the weighting factor between the accelerometer samples and the magnetometer samples (Lee and Park 2009). The number of functions must at least be as many as the number of states, thus the magnetometer and the accelerometer must be used in tandem.

A new better quaternion is found iteratively with the following steps.

$$J = \frac{\partial \begin{bmatrix} Q(q) & 0 \\ 0 & Q(q) \end{bmatrix} \begin{bmatrix} \mathbf{y}_{acc} \\ \mathbf{y}_{mag} \end{bmatrix}}{\partial q_j}; j = 0, 1, 2, 3 \quad (4.23)$$

$$\Delta q = (J^T J)^{-1} J^T \epsilon(q) \quad (4.24)$$

$$q^{i+1} = q^i - \Delta q \quad (4.25)$$

The new quaternion must then be normalized

$$q = q / \|q^{i+1}\| \quad (4.26)$$

Equations (4.23) to (4.26) are repeated until convergences. The definition used for convergences here is that the quaternion correction is smaller than a given threshold, or a maximum amount of iterations is reached. Experiments have concluded that 3 iterations are typically sufficient.

$$\Delta q \leq \xi \text{ OR } i \geq a$$

Depending on whether the magnetometer and accelerometer vectors fulfill certain criteria, three different inputs are given to the G-N algorithm. If both the accelerometer and magnetometer vectors are deemed undisturbed, both are sent in as input. If only the accelerometer vector fulfills them, a "fake" magnetometer vector is calculated as

$$\mathbf{Z}_A = T(q)^T \mathbf{h} \quad (4.27)$$

and provided together with the accelerometer vector to the algorithm. If instead only the magnetometer vector fulfills its criteria, a fake accelerometer vector is calculated as

$$\mathbf{Z}_M = T(q)^T \mathbf{g}. \quad (4.28)$$

Kalman Filter Formulation

Now that the measurements are represented in the same form as the orientation state, the quaternion from the measurement update of the Kalman filter becomes less complicated. However, the selection of the measurement covariant noise matrices is less obvious.

$$\begin{aligned} x_1 &= z_1 \\ x_2 &= z_2 \\ x_3 &= z_3 \\ x_4 &= z_4 \end{aligned} \quad (4.29)$$

$$H = eye(4) \quad (4.30)$$

$$\begin{aligned} R_{acc} &= eye(4) * C_1 \\ R_{mag} &= eye(4) * C_2 \end{aligned} \quad (4.31)$$

The measurement noise covariance matrices are simply selected as identity matrices with identical constant values, eq. (4.31). The H matrix is simply a 4 x 4 identity matrix. The discrete Kalman filter equations can be expressed as

$$\begin{aligned}x_{k+1} &= f(x_k, u_k) + w_k = Fx_k + w_k \\z_k &= h(x_k) + v_k = Hx_k + v_k\end{aligned}\tag{4.32}$$

4.6 Complementary Filter

The implementation of the complementary filter calculates the orientation using the gyroscope and the accelerometer alone. Similar to the Kalman filter it can be divided into two steps, a prediction step and a measurement step using the gyroscope and the accelerometer measurements, respectively. Thus, from the prediction step a quaternion is given. It is then converted to Euler Angles which are then weighed together with the ones calculated from accelerometer measurements. Given that the accelerometer is not exposed to any changes in velocity, and using the Aerospace Sequence the angles obtained from the measurements, the elevation ϕ and bank θ , are calculated as

$$\phi_{acc} = \sin^{-1} \left(\frac{a_x}{|\mathbf{a}|} \right)\tag{4.33}$$

$$\theta_{acc} = \sin^{-1} \left(\frac{-a_y}{|\mathbf{a}| \cos(\phi)} \right)\tag{4.34}$$

The gyroscope has low-frequency noise components and the accelerometer high-frequency noise components, thus, they are high-pass respectively low-pass filtered. The low-pass filter is denoted as $G(s)$ and subsequently the high-pass filter is $1 - G(s)$.

$$\phi = (1 - G(s))\phi_{gyro} + G(s)\phi_{acc}\tag{4.35}$$

$$\theta = (1 - G(s))\theta_{gyro} + G(s)\theta_{acc}\tag{4.36}$$

After this step the angles are converted back to a quaternion that is used in the next iteration.

Some problems with this method exist. The Euler angles have singularity issues around certain angles, and the angles in the averaging equations (4.35,4.36) must be presented in the same region to get a proper average. These issues can be taken care of, or the problematic regions best be avoided.

To validate that the zero acceleration assumption is true, or relatively true, an accelerometer outlier detector is used. For the case that this is not fulfilled the low-pass filter gain is set to zero, $G(s) = 0$.

4.7 Outlier Detection

The fact that the measurement updates depend on relatively pure measurements of the gravitational force and the Earth's magnetic field, outlier detection is needed. The outlier detector checking the accelerometer measurements sifts away all but the samples that contain a low portion of external acceleration, and the magnetometer outlier detector take away samples in which it detects interfering magnetic fields. A description of the outlier detectors the filters can use is presented below.

The total magnitude of the acceleration is compared with the well-known gravitational vector's norm. The threshold, ϵ_{acc} is derived from an accelerometer test in which the device was in a fixed position and the variance of the magnitude was calculated. ϵ_{acc} is set to a test decided factor of that variance.

$$|\sqrt{a_x^2 + a_y^2 + a_z^2} - |\mathbf{g}|| < \epsilon_{acc}$$

$$\epsilon_{acc} = n \cdot var(\sqrt{a_x^2 + a_y^2 + a_z^2})$$

The three outlier detection methods for the magnetometer described in the theory chapter were implemented. The first, which looks at the magnitude, and the second, which looks at the Dip Angle, were implemented exactly as they are described in Eq. 3.12 and in Eq. 3.14. The $\bar{\lambda}$ calculated by Eq. 3.16 was used to calculate a value

$$W = e^{-\bar{\lambda}^2/s} \quad (4.37)$$

and then this value was compared to a threshold

$$W > \epsilon_{mag,3}. \quad (4.38)$$

Equation 4.37 is used by (Callmer *et al.* 2013) as a weighting function but is here only used to more easily detect differences between values of $\bar{\lambda}$. The parameters of the different outlier detectors were tuned so that the detectors all removed the same amount of samples.

4.8 Mapping

Unfortunately, the lack of reliable absolute measurements of the heading angle will inevitably lead to a positional drift over time. This drift has to be reduced if the system is to be used in any real application. One step toward that end is to utilize information about the physical surroundings, that is, floor maps. To do that, a mapping algorithm intended to be used in conjunction with the output from the three PDR systems was created and implemented. A flow diagram of the entire IPS is shown in Figure 4.6.

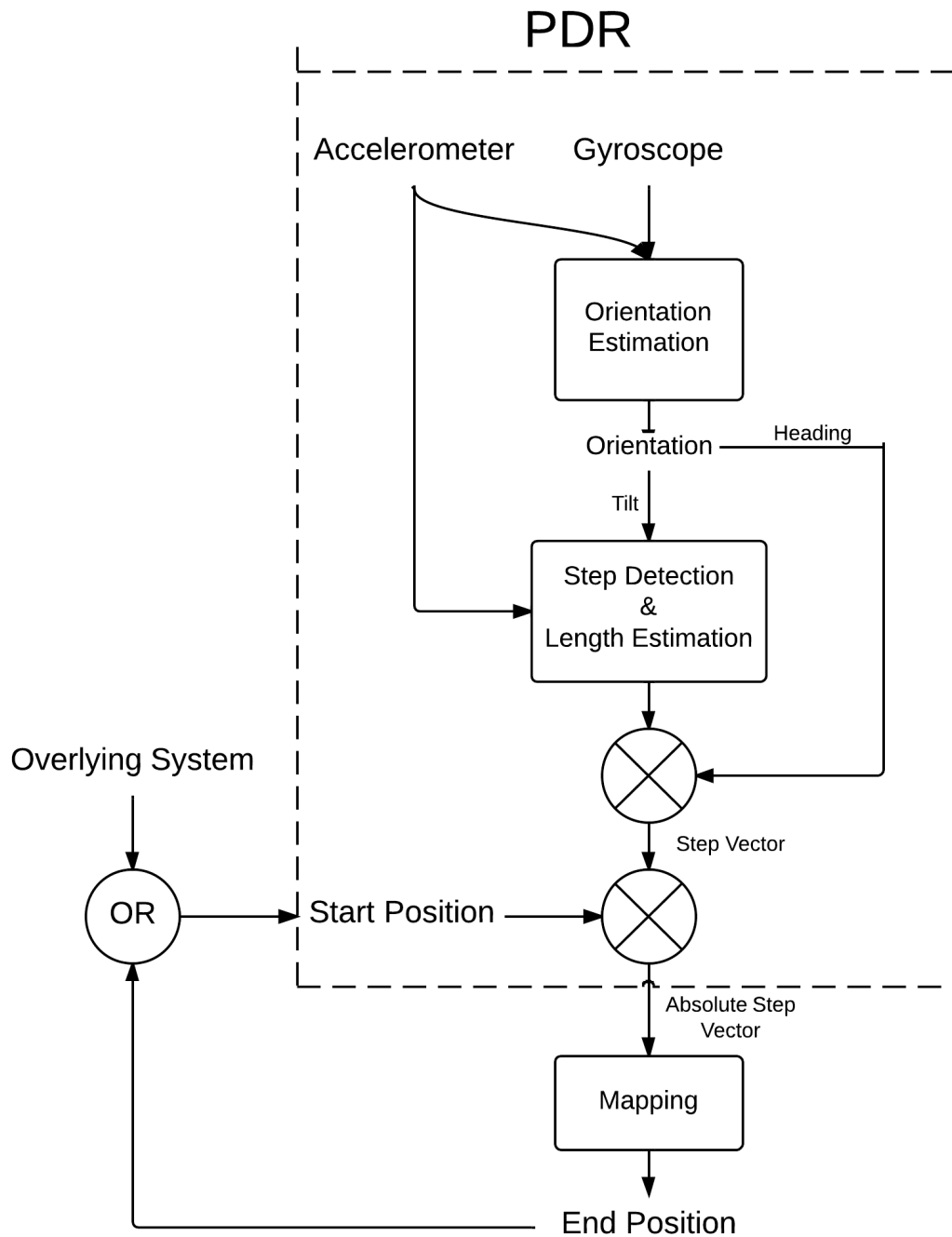


Figure 4.6. An overview of the entire system, with both the PDR system and the mapping algorithm.

Given a start position on the map the algorithm checks certain conditions each step. Specifically, it checks whether the step vector intersects with an obstacle. The only obstacles considered here were walls. If the vector does intersect at some point

with a wall, one of two actions will be taken - depending on the angle of incidence, denoted as α , between the vector and the wall. It should be mentioned that the mapping algorithm was implemented in this project so that it and the orientation estimation algorithm ran separately. That is, the orientation estimation was done on an entire set of data from a walk, and then the mapping algorithm was added to the output of the orientation estimation. The corrections that were made on the heading angle were not sent back to the filter to update any states.

1. If the angle is smaller than a certain threshold, move away from the wall and adjust the heading angle so that updated the step vector becomes closer to being parallel to the wall.
2. If the angle is greater than a certain threshold, assume that the person has walked through a door into another room and change the position of the end of the step accordingly.

The two cases are depicted in Figure 4.7.

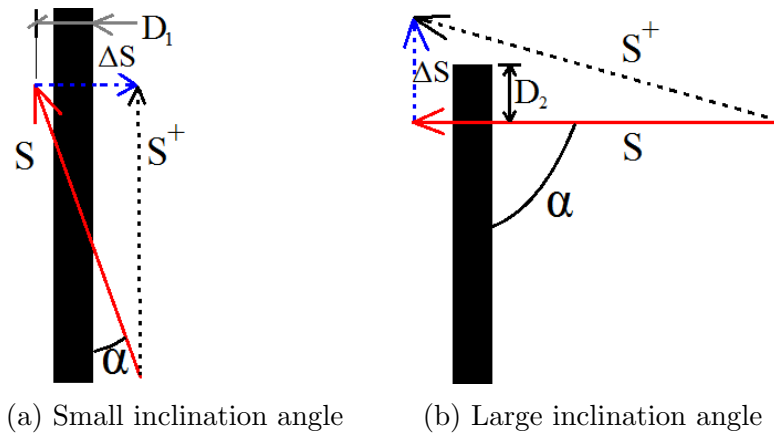


Figure 4.7. The red arrow depicts the original step vector, the blue arrow the change in position, and the black arrow the step vector after mapping. The angle ψ determines what measure to take.

Mathematically put, the updated heading provided by the first corrective action can be expressed by

$$\Psi^+ = \Psi + \Delta\Psi \quad (4.39)$$

where

$$\Delta\Psi = C_\Psi \alpha. \quad (4.40)$$

The sign of α varies with the type of collision and C_Ψ is a constant which is contained within the interval $0 < C < 1$.

The new step vector becomes

$$S^+ = S + \Delta S \quad (4.41)$$

wherein

$$|\Delta S| = D_1 + C_{S,1} \quad (4.42)$$

and the direction of ΔS is parallel to the wall's normal, D_1 is the distance to the other side of the wall, and $C_{S,1}$ is a tuning parameter.

In the second case, the heading is left untouched. The new step vector becomes, like the first case

$$S^+ = S + \Delta S \quad (4.43)$$

but with

$$|\Delta S| = D_2 + C_{S,2}. \quad (4.44)$$

The direction of ΔS is parallel to the wall, D_2 is the distance to the opening, and $C_{S,2}$ is a tuning parameter.

For clarification, when the heading angle is corrected, all subsequent heading angles are as well. This means that the first type of collision can correct a drift in heading while the second is not used to that end but instead only to correct positions.

5 RESULTS

The system's performance was evaluated by running it and its sub-systems on data from numerous tests. To evaluate the three orientation filters' performance, tests in which the device was rotated in various ways were carried out. There was no accurate reference in these tests, though, and for that reason the filters could only be evaluated relative to each other. Different outlier detection methods for the magnetometer signal were evaluated. The Step Detection and Length Estimation algorithm's performance was assessed by running it on data from tests during which a known distance, with a known number of steps, were walked. The PDR system was tested by providing it with data from repeated walks about the office floor of Ascom. The mapping algorithm was then applied the same data.

5.1 Orientation Estimation

The three filters were compared in tests during which the device was rotated about its axes in various ways. The Euler Angles were extracted from the output and plotted. Unfortunately, the testing equipment available was rather limited which led to a lack of an absolute reference in the tests. The equipment consisted of the iNemo module and the bare hands of the authors. The module was then rotated around its axes as controlled as can be expected with that equipment. Despite this, the results were worthy of being presented and analyzed.

In the test whose results are shown in Figure 5.1 and in 5.2 a complete revolution of the device around its y-axis was performed. The outputs of the Kalman and the G-N filter are almost identical in this test whereas that from the Complementary is significantly different. There is a larger discrepancy in the bank angles than in the elevation in the filter output.

In the test whose results are shown in Figure 5.3 the device's elevation angle was contained within the boundaries of the interval $[-\pi/2, \pi/2]$. In that test, and in other similar tests, the complementary filter appears to estimate the bank and elevation angles equally well as the other two filters.

The results of these tests shows that it is when the elevation angle goes beyond the limits of the interval $[-\pi/2, \pi/2]$ that the complementary filter's weaknesses become clear.

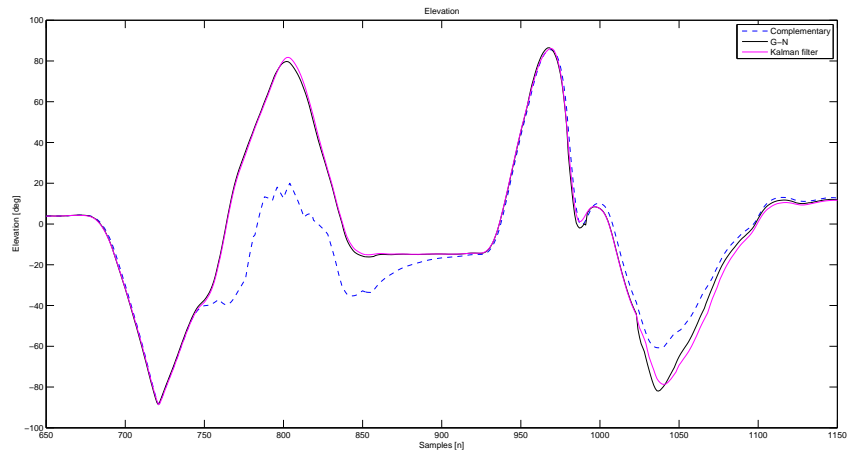


Figure 5.1. The elevation angles from the filters during a test.

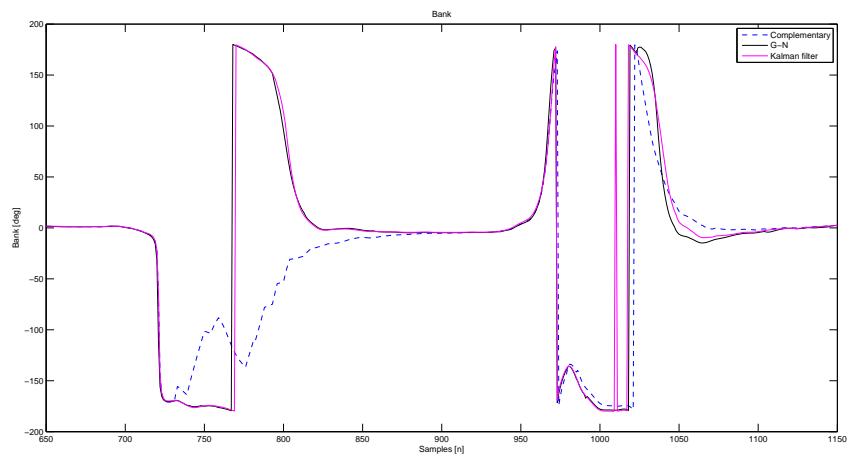


Figure 5.2. The bank angles from the filters during a test.

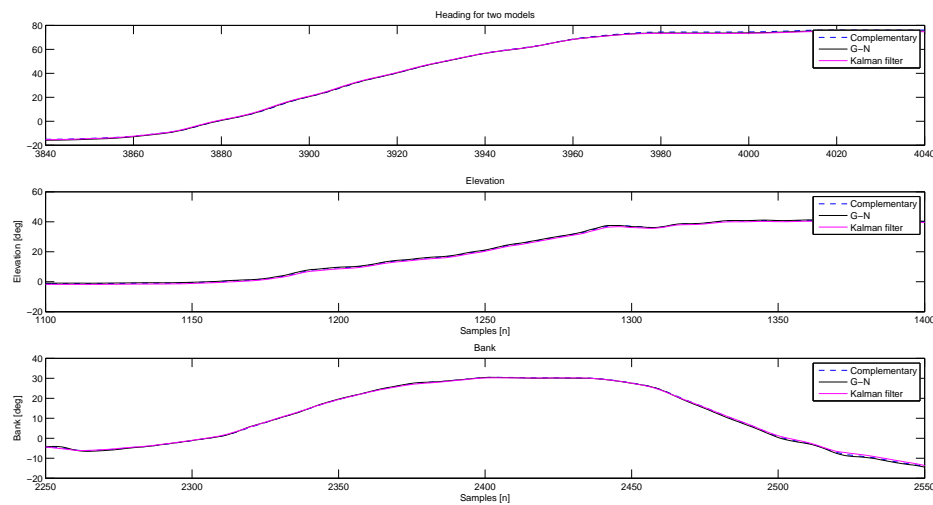


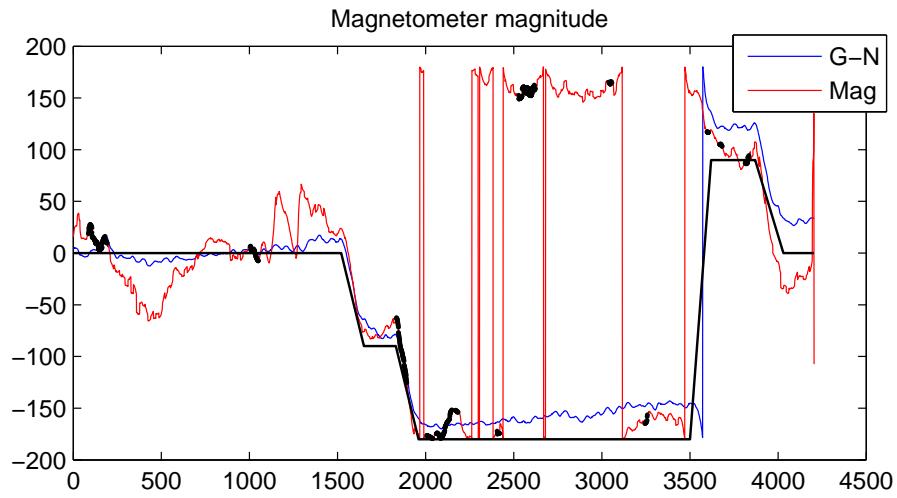
Figure 5.3. The heading, elevation, and bank angles of the filters' outputs from a test in which the device's elevation angle remained within the interval $[-\pi/2, \pi/2]$

5.2 Magnetometer Evaluation

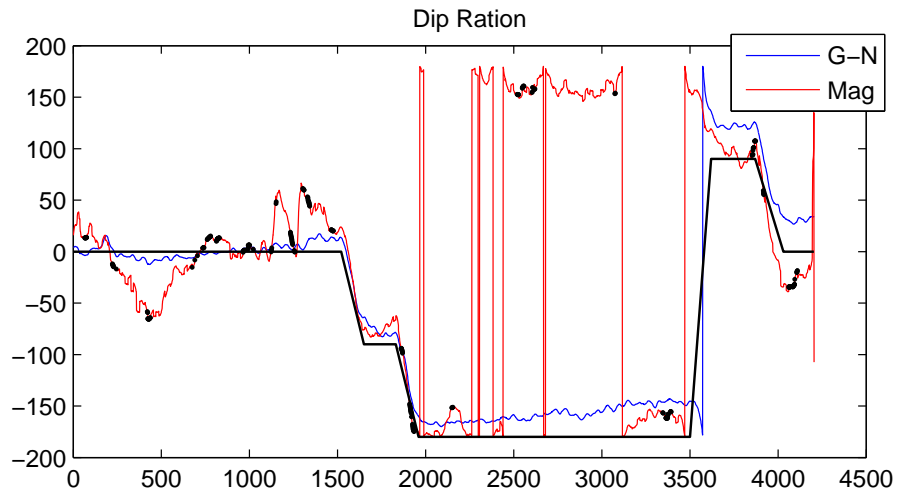
The different outlier detection methods were evaluated by testing them on data gathered from walks about the office floors of Ascom. In these rooms and hallways there are a vast number of electronic devices that emit magnetic fields which in turn shroud the Earth's magnetic field. If the outlier detectors successfully manage to discriminate the good measurements from the bad in these places, they are likely to work in many others as well. Due to time constraints, the magnetometer outlier detection models were not extensively evaluated. Only a small number of tests were carried out. They did, however, indicate that the third detection model was most successful at singling out the pure readings of the Earth's magnetic field from the distorted others.

The plots in Figure 5.4 are made from data gathered from one walk around the first floor of Ascom's C-building. The lap was walked in a counter-clockwise direction. During this test the device was held in the hand and its x-axis was pointing in the direction of the gait. The samples the detectors deem good are marked with black dots in the plots. The three plots do, like other tests, also suggest that the angular rate difference between the magnetometer and gyroscope is the best indicator of whether the readings are disturbed or not.

The third detection model, the angular rate model, was evaluated further by applying it to data from 8 clockwise walks about the first floor of Ascom's C-building. The results suggest that at the first half of the lap it reduces the accuracy of the estimated position and heading. However, after having walked some distance, about



(a) Magnitude of the magnetometer's measurement vector



(b) Dip ratio of the magnetometer's vertical and horizontal measurements

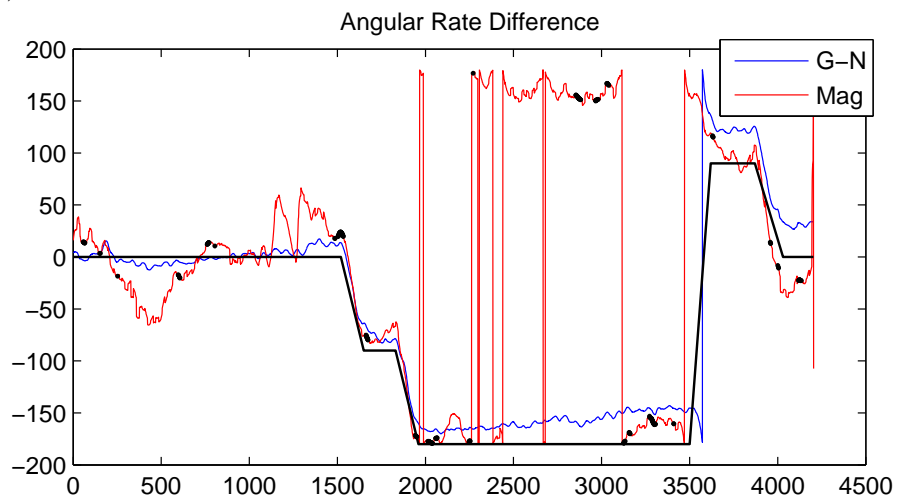
(c) Comparing angular rate $\sum_{i=-N/2}^{N/2} |\delta_i|$

Figure 5.4. The true heading is shown as a black line.

half of the lap, it begun to improve the accuracy of the estimate of the heading angle. This is expected due to that the drift from the gyroscope is relatively small short term, but it increases with time. The magnetometer's errors are not time dependent though, so eventually, at a certain break even time instant, the magnetometer's accuracy surpasses that of the gyroscope. In addition to that, it seems most of the good magnetic readings occur at the later parts of the lap. It is reasonable to expect that some locations are less disturbed than others, which is probably the case on the floor these tests were carried out on. The trajectories from these tests are shown in Figure 5.5. The average heading errors and its variance is presented in Table 5.1

Table 5.1. Statistical results from the eight magnetometer evaluation tests. The G-N filter was run with and without the magnetometer measurement update activated.

	Average Heading error	Variance Heading error
G-N	6.22°	0.063°
Magnetometer	6.87°	0.21°



Figure 5.5. .

5.3 Step Detection and Length Estimation

A distance of approximately 91.5 meters was walked eight times. The true number of steps, which was counted manually, and the true distance were compared to the estimated. The device was worn on the hip. The G-N based filter was used to transform the measured accelerations from the Device Frame to the World Frame. The step detection and length estimation algorithm was run on the data from those tests and the results are presented in Table 5.2.

Table 5.2. Results of the step detection and step length estimation. The mean error in steps counted and mean error in total length are presented.

	Mean	Variance
No. of steps	-1.88 steps	0.70 steps
Distance	-2.13 m	1.46 m

It seems the algorithm tends to underestimate the distance and the number of steps walked. Part of the loss in distance is probably due to the lost steps and part of it is probably due to a not perfectly tuned K -value, and imperfections in the model itself.

5.4 PDR System

The PDR system was further evaluated with data gathered from 10 walks about the office floor. The trajectory walked as well as the start and end positions were the same in all these tests. The device logging the data was worn on the hip during all tests. The magnetometer was not used. The heading errors for each model are presented in Table 5.3. The corresponding errors in position is presented in Table 5.4. Plots of some of the trajectories are presented in Figure 5.6.

Table 5.3. Results of the PDR system without mapping. The average heading error is the mean value of the deviation from the true trajectory's heading angle. The end heading error is the difference between the true end heading and the estimated.

	Average Heading error	End heading error
G-N	8.5°	27.2°
Kalman	8.7°	27.8°
Complementary	10.3°	23.9°

Table 5.4. Results of the PDR system without mapping. The average position error is the mean value of the deviation from the true trajectory's position. The end position error is the difference in distance between the start and estimated end position for tests 1-10.

	Average position error	End position error
G-N	1.6 m	3.0 m
Kalman	1.7 m	3.4 m
Complementary	1.8 m	3.2 m

5.5 Mapping

The entire system, with mapping activated, was evaluated with the same data the PDR system were.

Table 5.5. Same as Table 5.3 but with mapping activated.

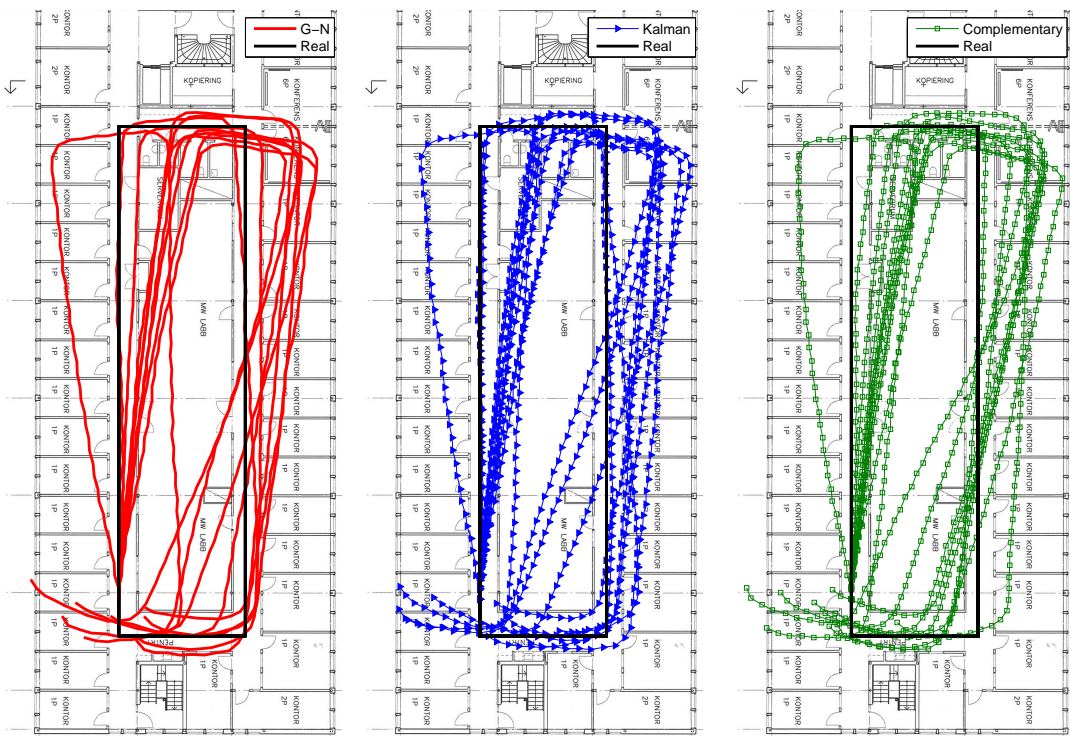
	Average Heading error	End heading error
G-N (mapping)	5.1°	36.1°
Kalman (mapping)	5.3°	37.5°
Complementary (mapping)	5.2°	36.8°

Table 5.6. Same as Table 5.4 but with mapping activated.

	Average position error	End position error
G-N (mapping)	0.52 m	3.2 m
Kalman (mapping)	0.51 m	3.1 m
Complementary (mapping)	0.50 m	3.2 m

It is clear from the statistics presented in the Tables 5.3 to 5.6, and from the plots in Figure 5.6, that the trajectories are improved greatly when mapping is used. They also suggest that the G-N based filter has a slightly better performance, primarily in the average heading error without mapping.

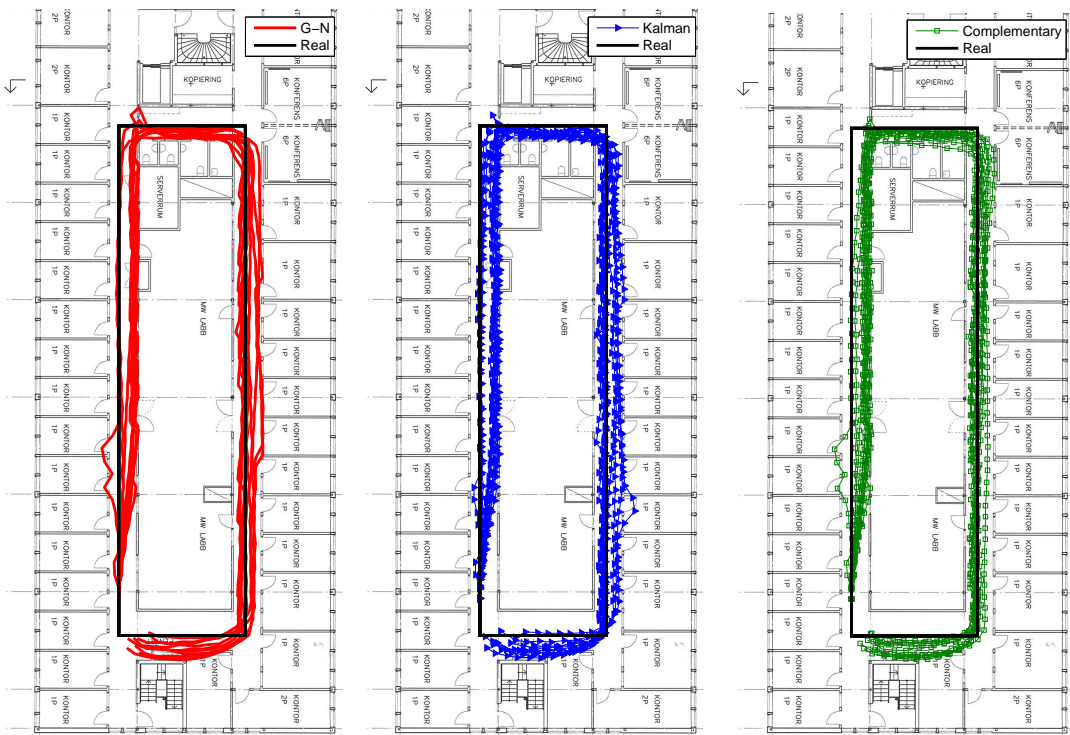
The mapping algorithm, though, does not always work as intended. And when it does not, which is rare, the trajectory can sustain seemingly irreparable damage. Such an example is seen in Figure 5.7.



(a) G-N

(b) Kalman

(c) Complementary



(d) G-N (mapping)

(e) Kalman (mapping)

(f) Complementary (mapping)

Figure 5.6. Trajectories of the different filters for 10 tests.

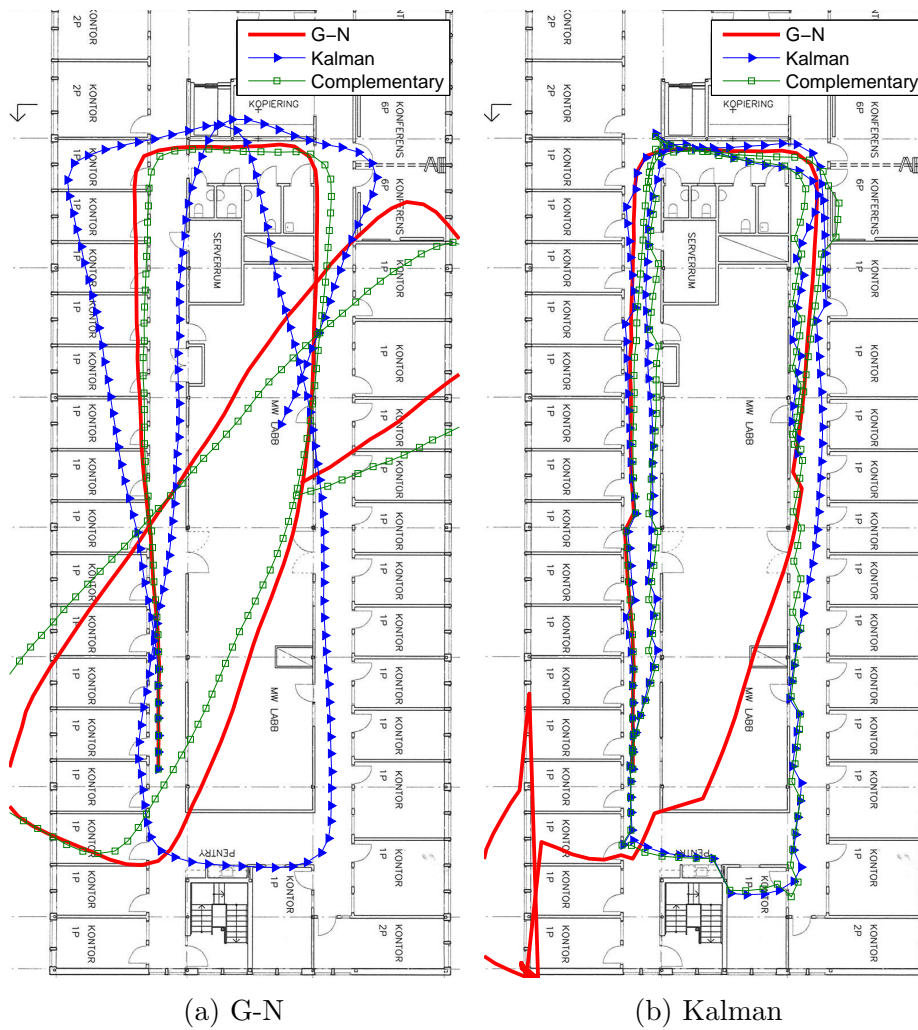


Figure 5.7. A test where the mapping algorithm loses track of the true trajectory after the PDR system incorrectly claims that the person has walked into the large room in the middle.

6 DISCUSSION

Although it is clear from the results that no one of the three PDR systems, when used alone, have the accuracy the more security critical applications require, they can serve as sound bases for IPSs using them in conjunction with other technologies. The results show that even a rather modest mapping algorithm renders the trajectories much more pleasant to behold. If further information from IR-beacons or wireless Bluetooth networks were to be added, an even higher precision could be achieved. The three filters show a very similar performance in the tests, but there are reasons why the G-N and Kalman filters are to be preferred to the complementary. They operate completely in the domain of quaternions which means that they avoid the problems Euler Angles are associated with. It is also advantageous not having to go back and forth between different representations of the orientation for computational reasons. However, since the heading angle, an Euler Angle, is extracted from the orientation provided by each filter, the Euler Angle representation is never, by the whole PDR system, completely avoided.

In some buildings in which there are large open spaces, for example in warehouses, mapping cannot be relied upon so heavily. Then, the accuracy of the orientation estimation becomes more critical. To determine which filter performs the best, more tests would have to be conducted. If their performance is deemed indistinguishable, their computational requirements instead become the deciding factor. The G-N algorithm can be re-written to reduce its computational requirements (Lee and Park 2009). The Kalman filter can probably also be re-formulated and optimized, but to what extent is unknown to the authors. For these reasons, it is hard to conclude which filter is the best.

Calibrating the sensors better, and possibly doing it as the filters are running, could improve the accuracy. The covariance matrices of the Kalman and G-N filters could also probably be approximated better. Doing that could lead to a larger discrepancy between the Kalman based filters and the complementary.

For buildings wherein there are many walls, the magnetometer will most likely not improve the accuracy of the system if a mapping algorithm already corrects the drift in heading. It should be stressed, however, that the full potential of the magnetometer has most likely not been utilized by the system created in this project. A more effective and adaptive disturbance detector could invalidate the statement that the magnetometer would not improve the system's accuracy. One such detector could potentially use a combination of the different outlier detection methods described here and/or utilize the characteristics of the disturbances. Moreover, as mentioned above, mapping cannot be used everywhere to the same extent it has on the data from the tests done in this project. For applications that are intended to be used in such places, a system in which the magnetometer is successfully incorporated is most likely more suitable than one heavily relying on mapping. It could also be used to initialize the PDR system, that is, it could give a starting heading. But

if the magnetometer is to give absolute measurements of the person's heading, its orientation in relation to that person has to be estimated as well.

More advanced mapping algorithms could potentially increase the precision and robustness of the IPS further yet. Mapping puts higher demands on the accuracy of the step length estimation, however. Due to that, it is motivated to further develop and/or evaluate other step length and detection models. The mapping algorithm described here somewhat alters the step length when making corrections, which is undesirable. More advanced mapping algorithms, relying on statistical models, can even eliminate, or greatly reduce, the need of an initial heading or position.

In conclusion it can be said that the PDR system created in this project does what it is supposed to, that is, give positional information in-between updates from overlying systems. Further work has to be done to increase its robustness with respect to user habits. It is the authors' firm belief that the greatest potential of improvement lies within mapping. With the PDR system presented here, a robust mapping algorithm, and the occasional update from beacons, a precision sufficient for even the more critical applications can be achieved.

Bibliography

- Attia, Mohamed, Moussa, Adel and El-Sheimy, Naser (2013). Map aided pedestrian dead reckoning using buildings information for indoor navigation applications. *Positioning*, **4**(3), 227–239.
- Bissig, P., Wattenhofer, R. and Welten, S. (2013). A pocket guide to indoor mapping. In: *Positioning Navigation and Communication (WPNC), 2013 10th Workshop on*. pp 1–6.
- Blanke, Ulf and Schiele, Bernt (2008). Sensing location in the pocket.. In: *10th Int. Conference on Ubiquitous Computing (UbiComp, adjunct proceedings)*. no publisher. Seoul, South Korea. pp 1–2.
- Callmer, Jonas, Tornqvist, David and Gustafsson, Fredrik (2013). Robust heading estimation indoors using convex optimization. ISIF (Intl Society of Information Fusi. pp 1173–1179.
- Castaneda, N. and Lamy-Perbal, S. (2010). An improved shoe-mounted inertial navigation system. In: *Indoor Positioning and Indoor Navigation (IPIN), 2010 International Conference on*. pp 1–6.
- Chen, Wei, Chen, Wei, Chen, Ruizhi, Chen, Ruizhi, Chen, Yuwei, Chen, Yuwei, Kuusniemi, Heidi, Kuusniemi, Heidi, Wang, Jianyu and Wang, Jianyu (2010). An effective pedestrian dead reckoning algorithm using a unified heading error model. *IEEE*. pp 340–347.
- Davidson, Pavel, Davidson, P., Collin, Jussi, Collin, J., Takala, Jarmo and Takala, J. (2010). Application of particle filters for indoor positioning using floor plans. *IEEE*. pp 1–4.
- Evennou, Frederic and Marx, Francois (2006). Advanced integration of wifi and inertial navigation systems for indoor mobile positioning. *EURASIP Journal on Advances in Signal Processing*, **2006**(1), 086706.
- Fang, Lei, Antsaklis, P.J., Montestruque, L.A., McMickell, M.B., Lemmon, M., Sun, Yashan, Fang, Hui, Koutroulis, I., Haenggi, M., Xie, Min and Xie, Xiaojuan (2005). Design of a wireless assisted pedestrian dead reckoning system - the navmote experience. *Instrumentation and Measurement, IEEE Transactions on*, **54**(6), 2342–2358.
- Faulkner, W. Todd, Alwood Robert Taylor David W.A. Bohlin Jane (2010). Gps-denied pedestrian tracking in indoor environments using an imu and magnetic compass. *Proceedings of the 2010 International Technical Meeting of The Institute of Navigation, San Diego, CA*, **54**(6), 198–204.
- Foxlin, E. (2005). Pedestrian tracking with shoe-mounted inertial sensors. *Computer Graphics and Applications, IEEE*, **25**(6), 38–46.

- Gauss, Carl F. (1857). *Theory of the motion of the heavenly bodies moving about the sun in conic sections: a translation of Gauss's "Theoria motus."* With an appendix. By Charles Henry Davis.
- Gauss, Carl Friedrich (2014). The intensity of the earth's magnetic force reduced to absolute measurement. <http://21stcenturysciencetech.com/translations/gaussMagnetic.pdf>.
- Godha, S. and Lachapelle, G. (2008). Foot mounted inertial system for pedestrian navigation. *Measurement Science and Technology*, **19**(7), 075202.
- Harle, R. (2013). A survey of indoor inertial positioning systems for pedestrians. *Communications Surveys Tutorials, IEEE*, **15**(3), 1281–1293.
- Ichikawa, F., Chipchase, J. and Grignani, R. (2005). Where's the phone? a study of mobile phone location in public spaces. In: *Mobile Technology, Applications and Systems, 2005 2nd International Conference on*. pp 1–8.
- Jay Esfandyari, Roberto De Nuccio, Gang Xu (2010). Introduction to mems gyroscopes.
- Jimenez, A.R., Seco, F., Prieto, C. and Guevara, J. (2009). A comparison of pedestrian dead-reckoning algorithms using a low-cost mems imu. In: *Intelligent Signal Processing, 2009. WISP 2009. IEEE International Symposium on*. pp 37–42.
- Judd, T. and Vu, Toan (2008). Use of a new pedometric dead reckoning module in gps denied environments. In: *Position, Location and Navigation Symposium, 2008 IEEE/ION*. pp 120–128.
- Jussi Collin, Oleg Mezentsev, Grard Lachapelle (2003). Indoor positioning system using accelerometry and high accuracy heading sensors.
- Kang, Wonho, Nam, Seongho, Han, Youngnam and Lee, Sookjin (2012). Improved heading estimation for smartphone-based indoor positioning systems. *IEEE*. pp 2449–2453.
- Kim, A. and Golnaraghi, M. F. (2004). A quaternion-based orientation estimation algorithm using an inertial measurement unit. pp 268–272.
- Kopytoff, Verne (2013). Stores sniff out smartphones to follow shoppers. *MIT Technology Review*.
- Kouroggi, M., Ishikawa, T. and Kurata, T. (2010). A method of pedestrian dead reckoning using action recognition. In: *Position Location and Navigation Symposium (PLANS), 2010 IEEE/ION*. pp 85–89.
- Kuipers, Jack B. (1999). *Quaternions and rotation sequences : a primer with applications to orbits, aerospace, and virtual reality*. Princeton Univ. Press. Princeton, NJ.

- Kunze, Kai, Lukowicz, Paul, Junker, Holger and Trster, Gerhard (2005). Where am i: Recognizing on-body positions of wearable sensors. In: *In: LOCA04: International Workshop on Location and Context-Awareness*. Springer-Verlag. pp 264–275.
- Kwanmuang, Surat, Ojeda, Lauro and Borenstein, Johann (2011). Magnetometer-enhanced personal locator for tunnels and gps-denied outdoor environments.
- Lee, Jung Keun and Park, E.J. (2009). A fast quaternion-based orientation optimizer via virtual rotation for human motion tracking. *Biomedical Engineering, IEEE Transactions on*, **56**(5), 1574–1582.
- Lee, Seon-Woo, Mase, K. and Mase, K. (2002). Activity and location recognition using wearable sensors. *IEEE Pervasive Computing*, **1**(3), 24–32.
- Liu, Hui, Darabi, H., Banerjee, P. and Liu, Jing (2007). Survey of wireless indoor positioning techniques and systems. *Systems, Man, and Cybernetics, Part C: Applications and Reviews, IEEE Transactions on*, **37**(6), 1067–1080.
- Lu, Ming F., Liu, Bang C., Wu, Jian P., Hsu, Fu K. and Huang, Wen T. (2013). The indoor automatic guided vehicle with an ir positioning and low-cost inertial navigation system. *Applied Mechanics and Materials*, **300-301**, 494.
- Madgwick, S.O.H., Vaidyanathan, R. and Harrison, A.J.L. (2010). An efficient orientation filter for inertial measurement units (imus) and magnetic angular rate and gravity (marg) sensor arrays. Technical report. Department of Mechanical Engineering.
- Magnetic declination* (2014). http://geomag.nrcan.gc.ca/mag_fld/magdec-eng.php.
- Marins, J.L., Yun, X., Bachmann, E.R., Mcghee, R.B. and Zyda, M.J. (2001). An extended kalman filter for quaternion-based orientation estimation using marg sensors. In: *Intelligent Robots and Systems, 2001. Proceedings. 2001 IEEE/RSJ International Conference on*. vol. 4. pp 2003–2011 vol.4.
- NOAA, National Geophysical Data Center (2014). Estimated values of magnetic field. <http://www.ngdc.noaa.gov/geomag-web/>.
- Pedley, Mark (2013). Build and calibrate a tilt-compensating electronic compass.
- Roetenberg, Daniel (2006). Inertial and magnetic sensing of human motion. PhD thesis. Enschede.
- Sabatini, A. M. (2006). Quaternion-based extended kalman filter for determining orientation by inertial and magnetic sensing. *IEEE Transactions on Biomedical Engineering*, **53**(7), 1346–1356.
- ST (2010). Using lsm303dlh for a tilt compensated electronic compass.

- Steinhoff, U. and Schiele, B. (2010). Dead reckoning from the pocket - an experimental study. In: *Pervasive Computing and Communications (PerCom), 2010 IEEE International Conference on*. pp 162–170.
- Stella, M., Russo, M. and Begusi, D. (2012). Rf localization in indoor environment. *Radioengineering*, **21**(2), 557–567.
- Suh, Young-Soo and Park, Sangkyung (2009). Pedestrian inertial navigation with gait phase detection assisted zero velocity updating. In: *Autonomous Robots and Agents, 2009. ICARA 2009. 4th International Conference on*. pp 336–341.
- Terejanu, Gabriel A (2003). Extended kalman filter tutorial. *Online*. *Disponibile:* <http://users.ices.utexas.edu/~terejanu/files/tutorialEKF.pdf>.
- The Institute of Technology at Linkping University (2013). Orientation estimation using smartphone sensors. [Online; accessed 27-May-2014].
- Wang, Yong (2012). Gaussnewton method. *Wiley Interdisciplinary Reviews: Computational Statistics*, **4**(4), 415–420.
- Watanabe, T. and Minegishi, Y. (2009). A test of stride length measurement with an accelerometer and a gyroscope attached on the foot. vol. 25. pp 502–505.
- Weinberg, Harvey (2002). Using the adxl202 in pedometer and personal navigation applications.